Higgs boson couplings: Measurements and theoretical interpretation

Higgs boson couplings: measurements and theoretical interpretation

Chiara Mariotti*

INFN, Sezione di Torino, Italy

Giampiero Passarino†

Dipartimento di Fisica Teorica, Università di Torino, Italy
INFN, Sezione di Torino, Italy

This report will review the Higgs boson properties: the mass, the total width and the couplings to fermions and bosons. The measurements have been performed with the data collected in 2011 and 2012 at the LHC accelerator at CERN by the ATLAS and CMS experiments. Theoretical frameworks to search for new physics are also introduced and discussed.

Keywords: Higgs physics; Standard Model; Effective Field Theory.

12.60.-i11.10.-z14.80.Bn

*chiara.mariotti@cern.ch
†giampiero@to.infn.it

Contents

1. Introduction

In the Standard Model (SM) when the electroweak symmetry is broken via the so-called Brout-Englert-Higgs mechanism (BEH) [1,2,3,4,5], vector bosons and fermions acquire mass and a new elementary particle with spin zero and positive parity appears: the Higgs boson. The ATLAS and CMS collaborations (the two general-purpose experiments at LHC) announced in July 2012 the observation of a new resonance in diphoton and 4-leptons final states with a mass around 125 *GeV*, whose properties are, to date, compatible within the large uncertainties with the Higgs boson predicted by the SM [6,7].

The Higgs boson production and decay rates measured by ATLAS and CMS give a combined signal yield, relative to the Standard Model (SM) prediction, of 1.09 ± 0.11 [8]. The Higgs boson mass is very precisely measured, several decay modes have been observed with high significance (the $\bar{\mathrm{b}}\mathrm{b}$-mode is not far from reaching the sensitivity to be observed at 13 *TeV* center of mass energy). Gluon fusion and vector-boson fusion production modes have been observed, and VH and $\bar{\mathrm{t}}\mathrm{tH}$ are not too far to reach the sensitivity to be observed.

The early discovery is certainly based on two pillars: experimental analysis improvements and theory accuracy improvements. To understand how the last two conspired to allow for the Higgs discovery see Refs. [9,10].

The LHC data are consistent with the SM predictions for all the parameterisations considered. Therefore, after the LHC Run 1, the SM of particle physics has been completed, raising its status to that of a full theory. However, despite its successes, this standard theory has shortcomings vis-à-vis cosmological observations. At the same time, there is presently a lack of direct evidence for new physics phenomena at the accelerator energy frontier.

No matter what the LHC will uncover in the future, understanding the Higgs boson properties is a pillar of the present paradigm. Direct searches, thus possibly new physics, and precision measurements will have to be consistent with each other. The need for a consistent theoretical framework in which deviations from the SM predictions can be calculated is necessary. Such a framework should be applicable to comprehensively describe measurements in all sectors of particle physics, not only LHC Higgs measurements but also electroweak precision data, etc. By simultaneously describing all existing measurements, this framework then becomes an intermediate step toward the next SM, hopefully revealing the underlying symmetries.

This report will review the measurements of the Higgs boson properties, mass, width and couplings to fermions and bosons, that were performed with the data collected in 2011 and 2012 (i.e. the Run 1) at the LHC accelerator at CERN by the ATLAS and CMS experiment. It will then introduce a theoretical framework to search for new physics, while measuring the Higgs couplings with high precisions.

2. Higgs boson phenomenology: production and decay

This Section is not intended to provide a complete phenomenological profile of the Higgs boson but only to recapitulate few essential informations that are needed to understand the experimental results and their theoretical interpretations.

At the LHC, the production of the SM Higgs boson occurs via the following processes, listed in order of decreasing cross section at $7-8$ *TeV* center-of-mass energy in Tab. 1.

Table 1: Higgs boson production processes.

gluon fusion production	$gg \to H$	Fig. 1,a
vector boson fusion production	$qq \to qqH$	Fig. 1,b
associated production with a W boson	$qq \to WH$	Fig. 2,a
or with a Z boson	$pp \to ZH$	Figs. 2,a
including a small ($\sim 8\%$) but less precisely known contribution from	$gg \to ZH$	2,b and 2,c
associated production with a pair of top or bottom quarks	$qq, gg \to \bar{t}tH$ or $\to \bar{b}bH$	Fig. 3
associated production with a single top quark	$qg \to tH$	Fig. 4

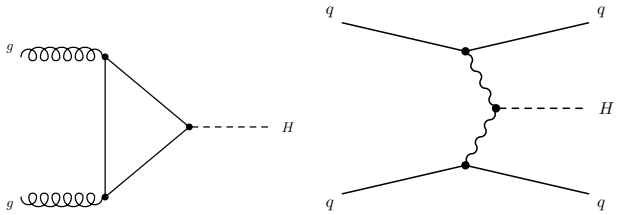

Fig. 1: Examples of leading-order Feynman diagrams for Higgs boson production via the (a) $gg \to H$ and (b) $qq \to qqH$ production processes.

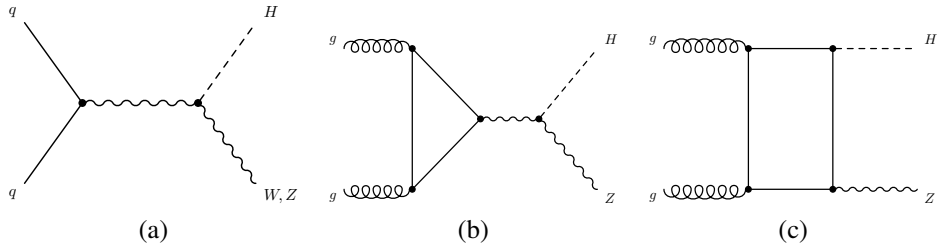

Fig. 2: Examples of leading-order Feynman diagrams for Higgs boson production via the (a) $qq \to VH$ and (b, c) $gg \to ZH$ production processes.

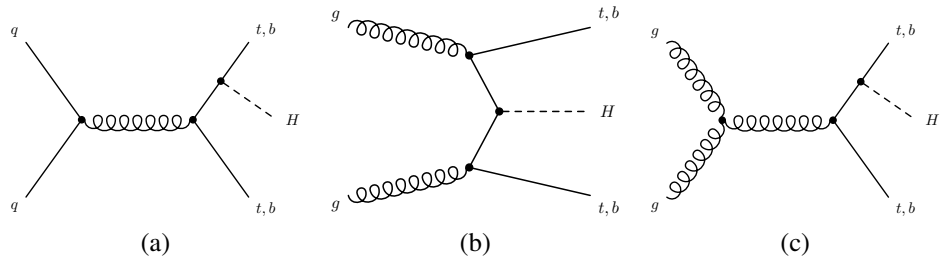

Fig. 3: Examples of leading-order Feynman diagrams for Higgs boson production in association with $\bar{\mathrm{t}}\mathrm{t}$ or $\bar{\mathrm{b}}\mathrm{b}$

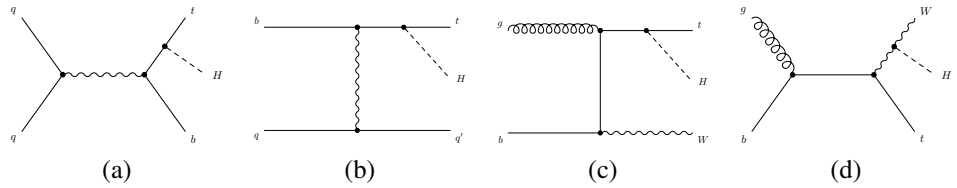

Fig. 4: Examples of leading-order Feynman diagrams for Higgs boson production in association with a single top quark.

The theory has an invariance based on the group $(2_{\mathrm{L}} \otimes 2_{\mathrm{R}}) = 1 \oplus 3$; the Higgs field, H, is the custodial singlet contained in a scalar doublet Φ of hypercharge $1/2$. The field Φ develops a vacuum expectation value (VEV) and H is the quantum fluctuation around the VEV. This has the consequence that the fermion masses and the Yukawa couplings are not independent quantities, i.e. H couples to a fermion-anti-fermion pair of the same flavour, with a coupling proportional to the mass of the fermion. Equivalently, H couples to vector boson (WW or ZZ) proportionally to their mass. This simple fact will have deep consequences when trying to build a model-independent framework for SM deviations.

In order to make the results of this Section transparent we stress the conceptual separation between diagrams, amplitudes, and (pseudo-)observables.

Diagrams, made of propagators and vertices, describe the couplings and the propagation and, in general, are not separately gauge invariant.

(Sub-)Amplitudes are a set of diagrams, e.g. the resonant (often called "signal") and the non-resonant (often called "background") parts of a physical process (which may contain more than one resonant part) and, once again, they are not separately gauge invariant.

Finally, (pseudo-)observables are elements (or are related to elements) of the S-matrix, e.g. partial decay widths or production cross sections. Therefore, for a light Higgs boson it makes sense to talk about $\mathrm{H} \to \mathrm{VV}$ or $\mathrm{H} \to \bar{\mathrm{f}}\mathrm{f}$ couplings, but objects like partial decay widths, e.g. $\Gamma_{\mathrm{H}\to\mathrm{VV}}$, (forbidden by kinematics) can only be given and interpreted within a certain set of conventions. Actually, it is not only a question of kinematics, H, W and Z

are unstable particles whose theoretical treatment is far from trivial and presents a certain number of subtleties [11,12]. Finally, a SM Higgs boson has a very narrow width, more than four orders of magnitude smaller than its mass, which means that theoretical "at the peak" predictions are provided in the so-called "zero-width-approximation" (ZWA), equivalent to (on-shell) production cross section $\times$ (on-shell) decay. In essence, the whole game in determining the Higgs couplings has to do with extracting vertices from (pseudo-)observables.

Having that in mind, the results presented below have been obtained as described below [9,10,13]. The Higgs total width resulting from `HDECAY` [14] has been modified according to the prescription:

$$\Gamma_{\mathrm{H}} = \Gamma^{\mathrm{HD}} - \sum_{\mathrm{V}=\mathrm{W},\mathrm{Z}} \Gamma^{\mathrm{HD}}_{\mathrm{V}} + \Gamma^{\mathrm{Pr}}_{4\mathrm{f}}, \tag{1}$$

where Γ_{H} is the total Higgs width, Γ^{HD} the Higgs width obtained from `HDECAY`, $\Gamma^{\mathrm{HD}}_{\mathrm{V}}$ stands for the partial widths to ZZ and WW calculated with `HDECAY`, while $\Gamma^{\mathrm{Pr}}_{4\mathrm{f}}$ represents the partial width of $\mathrm{H} \to 4\mathrm{f}$ calculated with `PROPHECY4F` [15]. The latter can be split into the decays into ZZ, WW, and the interference,

$$\Gamma^{\mathrm{Pr}}_{4\mathrm{f}} = \Gamma_{\mathrm{H}\to\mathrm{W}^*\mathrm{W}^*\to 4\mathrm{f}} + \Gamma_{\mathrm{H}\to\mathrm{Z}^*\mathrm{Z}^*\to 4\mathrm{f}} + \Gamma_{\mathrm{WW/ZZ-intf}}\,. \tag{2}$$

Whenever V^* appears it should be understood as follows: `PROPHECY4F` calculations are consistently performed with off-shell gauge bosons and they are valid above, near and below the gauge boson pair thresholds. For instance the definition is such that

$$\Gamma_{\mathrm{H}\to\mathrm{W}^*\mathrm{W}^*\to 4\mathrm{f}} = 9\,\Gamma_{\mathrm{H}\to\nu_{\mathrm{e}}\mathrm{e}^+\mu\bar{\nu}_\mu} + 12\,\Gamma_{\mathrm{H}\to\nu_{\mathrm{e}}\mathrm{e}^+\mathrm{d}\bar{\mathrm{u}}} + 4\,\Gamma_{\mathrm{H}\to\mathrm{u}\bar{\mathrm{d}}\mathrm{s}\bar{\mathrm{c}}}\,. \tag{3}$$

These conventions are essential in understanding every statement of the form "the H decays to W and Z bosons ...".

A complete generalisation is represented by the LHC-PO (where PO stands for pseudo-observables) framework [16,17,18,19]; the idea of POs has been formalised the first time in the context of electroweak observables around the Z pole at the LEP time [20]. A list of LHC POs will be introduced and discussed in Sect. 7.1. Suffice to mention here that the conditions defining POs ensure the generality of the approach and the possibility to match it to a wide class of new physics (NP) models. In brief, POs are experimentally accessible, well-defined from the point of view of QFT and capture all relevant effects of NP in the absence of new (non-SM) particles close to the Higgs mass.

Another useful definition concerns the "leading order": technically speaking leading-order (LO) defines the order in perturbation theory where the process starts. Notice that sometimes "LO" is used to denote tree level (as opposite to loops).

Examples of LO Feynman diagrams for the Higgs boson decays are shown in Figs. 5 and 6. The decays to W and Z bosons (see Fig. 5,a) and to fermions (see Fig. 5,b) start at tree level whereas the $\mathrm{H} \to \gamma\gamma$ decay starts at one loop, being generated by loops containing heavy quark or bosons, see Fig. 6.

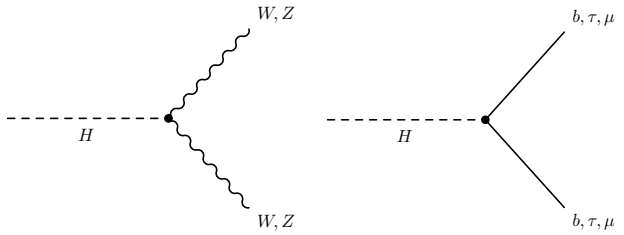

Fig. 5: Examples of leading-order Feynman diagrams for Higgs boson decays (a) to W and Z bosons and (b) to fermions (f = b, τ, μ).

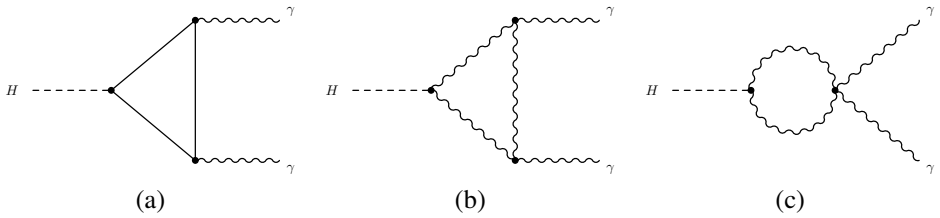

Fig. 6: Examples of leading-order Feynman diagrams for Higgs boson decays to a pair of photons.

The SM Higgs boson production cross sections and decay branching fractions have been calculated in the recent years at high order in perturbation theory. The many calculations have been compared and then eventually combined and summarised in Refs. [9,10,13], and they are shown in Figs. 7. Following these calculations, additional and important progress has been made, and many more calculations have been performed at higher order, but they will not be reported here, since they have not been used in the analysis of the Run 1 data. Once the mass of the Higgs boson has been measured, all its properties are fixed. The inclusive cross sections and branching fractions for the most important production and decay modes are summarised with their overall uncertainties in Tabs. 2 and 3 for a Higgs boson mass of 125.09 *GeV*, the value of the mass measured by the ATLAS and CMS collaboration with the Run 1 statistics [21].

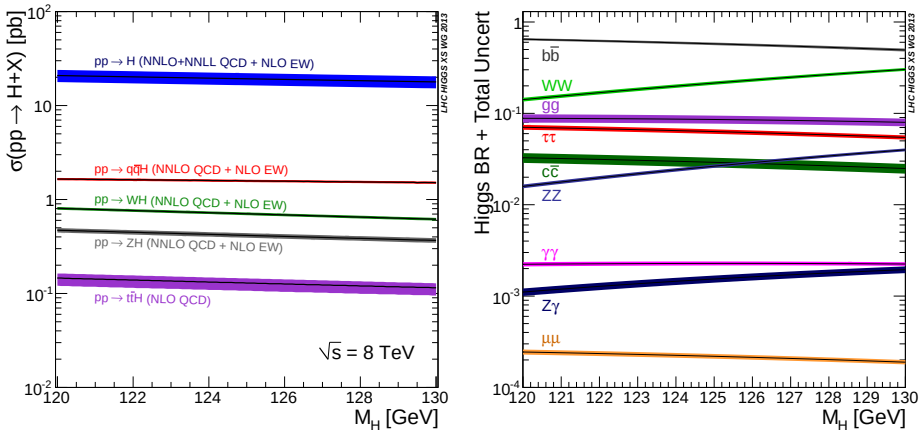

Fig. 7: Standard Model Higgs production cross sections and Branching Ratios at 8 *TeV* center of mass energy

Table 2: Standard Model predictions for the Higgs boson production cross sections together with their theoretical uncertainties as of the year 2013. The value of the Higgs boson mass is $m_{\mathrm{H}} = 125.09$ *GeV* as measured by the ATLAS and CMS experiments. The predictions are from Ref. [13]. The pp $\rightarrow$ ZH cross section, calculated at NNLO in QCD, includes both the quark-initiated, i.e. qq $\rightarrow$ ZH or qg $\rightarrow$ ZH, and the gg $\rightarrow$ ZH contributions. The uncertainties in the cross sections are evaluated as the sum in quadrature of the uncertainties resulting from variations of the QCD scales, parton distribution functions, and α_s. The uncertainty in the tH cross section is calculated following the procedure of Ref. [22]. The order of the theoretical calculations for the different production processes is also indicated in the table. In the case of $\mathrm{b\bar{b}H}$ production, the values are given for the mixture of five-flavour (5FS) and four-flavour (4FS) schemes as recommended in Ref. [23].

Production process	Cross section [pb] $\sqrt{s} = 7$ TeV	Cross section [pb] $\sqrt{s} = 8$ TeV	Order of calculation
ggF	15.0 ± 1.6	19.2 ± 2.0	NNLO(QCD) + NLO(EW)
VBF	1.22 ± 0.03	1.58 ± 0.04	NLO(QCD+EW) + *approx* NNLO(QCD)
WH	0.577 ± 0.016	0.703 ± 0.018	NNLO(QCD) + NLO(EW)
ZH	0.334 ± 0.013	0.414 ± 0.016	NNLO(QCD) + NLO(EW)
ggZH	0.023 ± 0.007	0.032 ± 0.010	NLO(QCD)
ttH	0.086 ± 0.009	0.129 ± 0.014	NLO(QCD)
tH	0.012 ± 0.001	0.018 ± 0.001	NLO(QCD)
bbH	0.156 ± 0.021	0.203 ± 0.028	5FS NNLO(QCD) + 4FS NLO(QCD)
Total	17.4 ± 1.6	22.3 ± 2.0	

Table 3: Standard Model predictions for the decay branching fractions of a Higgs boson with a mass of 125.09 GeV [21], together with their uncertainties [13].

Decay mode	Branching fraction [%]
Hbb	57.5 ± 1.9
HWW	21.6 ± 0.9
Hgg	8.56 ± 0.86
Htt	6.30 ± 0.36
Hcc	2.90 ± 0.35
HZZ	2.67 ± 0.11
$H\gamma\gamma$	0.228 ± 0.011
$HZ\gamma$	0.155 ± 0.014
$H\mu\mu$	0.022 ± 0.001

3. From discovery to properties

Before the 2012 discovery, the hypothesis was that the SM was the correct theory with $m_{\rm H}$ as the unknown parameter. Therefore, bounds on $m_{\rm H}$ were derived through a comparison of the SM theory with high-precision data [20]. At the LHC, after the discovery, the unknown parameters are the deviations of the measurements with respect to the SM predictions, given that the SM is fully specified and experimentally constrainable. Of course, the definition of SM deviations requires a characterisation of the underlying dynamics. Notice that, so far, all the available studies on the couplings of the new resonance conclude it to be compatible with the Higgs boson of the SM within present precision [24,25,8], and, as of yet, there is no direct evidence for new physics phenomena beyond the SM.

Best-fit results for the production signal strengths for the combination of ATLAS and CMS data are performed in the so-called kappa-framework. The next step will be to identify the optimal framework for SM deviations, i.e. a theory that will replace the kappa-framework after the experimental results will confirm a deviation.

We will introduce a few general definitions that will be relevant for understanding the experimental results and their interpretation. Technical details will be presented in the corresponding sections.

The kappa-framework The kappa-framework [26] introduced to parametrise SM deviations, is a procedure used at LO, partially accommodating factorisable QCD corrections (proportional to the SM LO) but not (the non-factorizable) electroweak (EW) corrections. It amounts to replace

$$\mathscr{L}_{\rm SM}\left(\{m\},\{g\}\right) \quad \text{with} \quad \mathscr{L}\left(\{m\},\{\kappa_g\, g\}\right), \tag{4}$$

where $\{m\}$ denotes the SM masses, $\{g\}$ the SM couplings and κ_g the scaling parameters. This is the framework used during Run 1.

The EFT/SMEFT Exact non-perturbative solutions to quantum field theories are rarely known and approximate solutions that expand observables perturbatively in a small coupling constant and in a ratio of scales are generally developed. Such quantum field theories can be regarded as examples of an effective field theory (EFT); the SM effective field theory (SMEFT) is an example. The theory is defined by

$$\mathscr{L} = \mathscr{L}_{\rm SM} + \sum_{n>4} \sum_{i=1}^{N_n} \frac{a_i^n}{\Lambda^{n-4}}\, \mathscr{O}_i^{(d=n)}, \tag{5}$$

with arbitrary Wilson coefficients a_i^n which, however, give the leading amplitudes in an exactly unitary S-matrix at energies far below the scale of new physics, Λ. The theory is (strictly) non-renormalisable, which means that an infinite number of higher dimensional operators must be included. Nevertheless, the amplitudes can be expanded in powers of $\mathrm{v}/\Lambda, E/\Lambda$, where v is the Higgs VEV and E is the typical scale at which we measure the process. The expansion is computable to all orders and ultraviolet divergencies can be cured

by introducing, order-by-order, an increasing number of counter-terms. A question that is often raised concerns the "optimal" parameterisation of the dim = 6 basis for the $\mathcal{O}_i^{(d=n)}$ operators; all sets of gauge invariant, dimension d operators, none of which is redundant, form a basis and all bases are equivalent. For a formal definition of redundancy see Sect. 3 of Ref. [27].

The rationale for constructing the SMEFT, i.e. an effective S-matrix $S^{\rm eff}(\Lambda)$, $\forall \Lambda < \infty$, has been described in Ref. [28]; the main assumption is that there is no fundamental scale above which $S^{\rm eff(\Lambda)}$ is not defined [29]. Of course, $S^{\rm eff}(\Lambda)$ loses its predictive power if a process at $E = \Lambda$ requires an infinite number of renormalized parameters [30]. The basis for NLO calculus of the SMEFT theory has been developed in Ref. [31] and in Refs. [32,33], see also Ref. [34].

When we compare SMEFT with kappa framework, it is worth noting that, even for QCD, there are contributions which induce sizeable corrections unrelated to the SM ones [35]. When considering the $H \to \bar{b}b$ decay, there are QCD corrections multiplying the SMEFT-modified amplitude which alter the vertex at LO but remain proportional to the SM ones, so NLO results can be obtained through a simple rescaling of the LO decay rate (i.e. equivalent to kappa framework). On the other hand, there are contributions which alter the LO vertex and induce sizeable corrections which are unrelated to the SM ones and cannot be easily anticipated.

We can conclude that, due to the absence of tantalising hints for new physics during Run 1 at LHC, the extension of the Higgs sector by dimension-six operators will provide a new standard for searches of non-resonant manifestations of the SM.

Phenomenological Lagrangians Any phenomenological approach, e.g. an extension of the SM Lagrangian with a limited number of interactions (like HVV and $H\bar{f}f$), is a reasonable starting point to describe limits on SM deviations. While this outcome is much less desirable than dealing with a consistent SMEFT, it is important to recognise that the difference relates to the possibility of including an estimate of the uncertainties induced by the truncation of the expansion. However, one has to mention that Monte Carlo tools are already available for phenomenological studies [36,37,38].

Pseudo Observables (POs) are a platform between realistic observables and theory parameters, allowing experimentalists and theorists to meet half way, without theorists having to run full simulation and reconstruction and experimentalists fully unfolding to model-dependent parameter spaces. Experimenters collapse some "primordial quantities" (say number of observed events in some pre-defined set-up) into some "secondary quantities" which we feel closer to the theoretical description of the phenomena. In other words, POs answer the question "how to store measurements in order to preserve them for a long time?" Indeed, the original kappa framework cannot explain many SM deviations, and Wilson coefficients in any EFT description are deeply rooted in a theoretical framework. Fiducial cross sections can be performed for a lot of bins. There is the need to extend the kappa parameters to something in between: theorists may refine their calculations and interpret

them against POs; if SM predictions improve experimentalist may redo POs [a].

To summarize, we can say that

- in the kappa framework, SM deviations are a simple rescaling of couplings and there are no new Lorentz structures; Higgs coupling fits are based on total rates.
- In the SMEFT there are new kinematical/Lorentz structures;
- phenomenological Lagrangians contain a subset of the interactions present in the SMEFT.

4. Analysis of the measurements

4.1. The final states

The following analyses have been performed in the ATLAS and CMS experiments to first discover and then to measure the Higgs boson properties:

$$\begin{array}{ll} H \to ZZ \to 4l & H \to \gamma\gamma \\ H \to WW \to l\nu l\nu & H \to \tau\tau^{+} \\ H \to b\bar{b} & H \text{ in association with } \bar{t}t \end{array}$$

The $H \to \mu^{-}\mu^{+}$ search has been also pursued in the experiments.

$H \to ZZ \to 4l$ [39,40] The signature for this final state is made of 4 electrons, or 4 muons, or 2 electrons and 2 muons of high p_T, isolated and coming from the primary vertex. The signal is reconstructed as a very narrow peak on top of a smooth background, composed by an irreducible part coming from the production of two non resonant Z bosons, and a reducible part from Z+jets and $\bar{t}t$ events, where jets are originating from heavy quarks, and thus could contain leptons, or are mis-identified as leptons.

The cross section of this process is tiny due to the small branching ratio of $H \to ZZ$ and even smaller branching ratios of $Z \to l^{+}l^{-}$, thus the analysis has to conserve the highest efficiency. The lepton identification and the lepton reconstruction are extremely pure and of high resolution, allowing to reach a m_H resolution of $1-2\%$.

Events within this channel are categorised as VBF-produced if there are 2 hight p_T jets, or as VH produced if there are additional leptons or V bosons, otherwise ggF produced.

$H \to \gamma\gamma$ [41,42] The signature for this final state is made by 2 energetic and isolated photons, that cluster in a narrow mass peak on top of a steeply falling spectrum. The background is composed mainly by an irreducible component from QCD production of 2 photons events and by a smaller contribution coming from γ+jets events, where a jet has

[a] A first public tool for POs is available at www.physik.uzh.ch/data/HiggsPO.

been mis-identified as a photon. A good fit and a good understanding of the shape of the background allow the analysis to be data-driven and not to rely on a perfect Monte Carlo simulation.

The analysis is very similar in the two experiments: the events are divided into categories of different expected signal-to-background ratio and on the presence or not of 2 jets of high invariant mass and high rapidity to select events produced through the Vector Boson Fusion (VBF) process. The candidate invariant mass is reconstructed with very good resolution of $1-2\%$.

$H \to WW \to l\nu l\nu$ [43,44,45] This is the channel with the highest cross-section. The mass reconstruction is not possible due to the presence of 2 neutrinos, and thus the background is hard to suppress and the signal has to be extracted from differences in shapes and from event counting. The 2 leptons are expected to have high p_T and small opening angle to conserve the V-A structure of the theory. The events have large missing transverse energy due to the presence of two high p_T neutrinos. The analysis is performed on exclusive jet multiplicity (0, 1, 2-jet) and considering also the presence of additional leptons, thus event categories can separate the different production modes.

The large background is studied in detail and all the components are estimated with data, after having obtained an enriched sample of that specific component. The Drell-Yan background is suppressed by cuts on the invariant mass of the 2 leptons, M_{ll}, and on the transverse missing energy, MET. Particular care has to be given to the MET since it is affected by the pile-up. The W+jets background (with one jet faking a lepton) is mitigated by a very pure and efficient ID. Background coming from top events is suppressed by the b-tag veto, or rejecting events with additional soft leptons. To partially subtract the irreducible WW background the M_{ll}, M_T (the lepton-neutrino transverse mass) and $\Delta(\phi)$ (the angle between the 2 charged leptons) distributions are used.

$H \to \tau^-\tau^+$ [46,47] The final state with two taus suffers from a low efficiency due to the relatively low p_T of the leptons coming from the τ decay, from the presence of at least 2 neutrinos from the decay and from the low $\tau^-\tau^+$ invariant mass resolution. The events are subdivided into jets categories: the 0-jet (that in CMS is used only to constrain the background), the 1-jet category, subsequently divided into a low p_T and a high p_T category, and the 2-jet categories targeting the VBF production mode. Thus the VBF, the VH and the ggF production modes can be separated. All the final states for the tau decays are considered in ATLAS, and a large fraction is analysed in CMS. The mass resolution is around $10-20\%$.

$H \to \bar{b}b$ [48,49] Due to huge background from $\bar{b}b$ QCD events, and due to the poor resolution of the $\bar{b}-b$ invariant mass (of the order of 10%) the ggF production mode in this final state cannot be considered inclusively. Thus the production mode with the highest signal-over-background is the VH one. In CMS a search of the Higgs boson decaying to $\bar{b}b$ produced in VBF has been carried out in Ref. [50], but the results have not been considered for the coupling analysis that will be presented in this review. Final states with zero additional leptons target the $ZH \to \nu\bar{\nu}b\bar{b}$ decay, with one high p_T lepton the $WH \to l\nu b\bar{b}$ decay

and with two high p_T leptons the $ZH \to llb\bar{b}$ decay.

H **produced in association with** $\bar{t}t$ [51,52,53,54,55] The final state with two top quark and a Higgs has a very small cross section, a broad spectrum of final states and as well as for the previous channel, a very large background. The final states with some clean signatures that help in separating the signal from the background are the following: the Higgs decaying into photons accompanied by 2 top quark signatures, and the Higgs decaying into WW, ZZ and $\tau\tau^+$, where final states with many leptons are selected. Although the cross section is not large enough to expect a significant observation, the measurements even with very large uncertainties play an important role in the Higgs boson coupling extraction.

$H \to \mu^-\mu^+$ [56,57] The search of the Higgs to $\mu\mu$ has been carried out in both experiments. Since the branching fraction in the Standard Model is very small, observing a signal would have been a hint for new physics. Upper limits have been set by both experiments.

5. The original kappa-framework

The original kappa-framework (OKF) has been introduced in Ref. [26] as a way to study deviations from the SM. To discuss the idea in general terms we consider a process involving the Higgs boson, e.g. $H \to \gamma\gamma$; the SM amplitude starts at one loop comprising fermion and bosonic contributions, i.e.

$$A^{SM}_{H\to\gamma\gamma} = A^{t}_{H\to\gamma\gamma} + A^{b}_{H\to\gamma\gamma} + A^{bos}_{H\to\gamma\gamma}\,, \tag{6}$$

where light fermions have been discarded. Each contribution is gauge parameter independent and proportional to the corresponding Higgs coupling. The idea is to modify Eq.(6) with ad hoc kappa parameters,

$$A^{\kappa}_{H\to\gamma\gamma} = \kappa_t\, A^{t}_{H\to\gamma\gamma} + \kappa_b\, A^{b}_{H\to\gamma\gamma} + \kappa_V\, A^{bos}_{H\to\gamma\gamma}\,, \tag{7}$$

and study their deviation from one. The formalism is simple but suffers of problems of consistency. Indeed, in a spontaneously broken gauge theory, masses and Yukawa couplings are not independent quantities. This fact is usually forgotten when dealing with massless fermions, typically in computing QCD corrections, but is the source of serious inconsistencies when higher-order EW corrections are included; altering the relation between masses and Yukawa couplings spoils the gauge invariance of the theory.

Furthermore, kinematics is not affected by the kappa parameters. Therefore the scheme works at the level of total cross-sections, not for differential distributions. In conclusion, the OKF is a LO construct, partially accommodating factorisable QCD corrections but not EW ones.

Implementation of the kappa framework Having in mind Eq.(7) as an example of the "theoretical" implementation of the OKF, we can briefly discuss how the framework is

implemented in practice in the experimental analysis. For a given production process or decay mode labelled by $\mathscr{O}^i$, a kappa parameter is defined such that

$$\kappa_i^2 = \frac{\mathscr{O}^i}{\mathscr{O}^i_{\rm SM}}\,, \tag{8}$$

giving $\kappa_i = 1$ in the SM. This defines $\mathscr{O}^i_{\rm SM}$ as SM equipped with the best available higher-order QCD and EW corrections, under the assumption that the dominant higher-order QCD corrections factorise.

Contributions from interference effects between the different (gauge invariant) sub-amplitudes provide some sensitivity to the relative signs of the Higgs boson couplings to different particles. Therefore, additional coupling modifiers are introduced, e.g. $\kappa_{\rm t}, \kappa_{\rm b}$, $\kappa_{\rm V}$ etc. In this way one has effective and resolved scaling factors, e.g. in gluon fusion we have

$$\text{effective} = \kappa_{\rm g}^2\,, \qquad \text{resolved} = \kappa_{\rm g}^2(\kappa_{\rm t},\kappa_{\rm b}) = 1.06\,\kappa_{\rm t}^2 + 0.01\,\kappa_{\rm b}^2 - 0.007\,\kappa_{\rm t}\,\kappa_{\rm b}\,, \tag{9}$$

where one should observe that, once again, the assumption of higher orders factorisation has been made. The generalisation for the resolved modifier case is shown in Eq.(49).

Underlying assumptions The OKF as any other framework that aims to study SM deviations is based on a certain number of additional assumptions. We consider only one Higgs doublet in the linear representation (a flexible choice) and the scalar doublet Φ (with hypercharge $1/2$) contains H, the custodial singlet in $(2_{\rm L}\otimes 2_{\rm R}) = 1\oplus 3$. Extensions are possible but "difficult", e.g. the two-Higgs doublet model (THDM) where

$$\Phi \to \Phi_i \qquad \Phi_i = {\rm R}_{ij}\,(\beta)\,\Psi^j\,, \tag{10}$$

with the technical hurdle of a diagonalisation of the mass matrix for the CP-even scalars.

New "light" degrees of freedom are not included and decoupling from heavy ones is a rigid assumption. To examine the consequences, consider the effect of heavy degrees of freedom in $\gamma\gamma \to {\rm H}$: to be fully general one has to consider effects due to heavy fermions and heavy scalars in arbitrary representations, R_f and R_s, of $SU(3)$ [58]. Colored scalars decouple from the low energy physics as their mass increases; however, the same is not true for fermions. To be more precise, besides decoupling we have other regimes: for a given amplitude containing a particle of mass m, in the limit $m\to\infty$, we have to distinguish three possible cases:

> Decoupling: ${\rm A}\sim 1/m^2$ (or more). The corresponding higher-order operators are called "irrelevant" ,
>
> Screening: ${\rm A}\to$ const (or $\ln m^2$). The operators are called "marginal" ,
>
> Enhancement: ${\rm A}\sim m^2$ (or more). The operators are called "relevant" .

It is worth noting that whenever the LO ρ-parameter [59] is different from one, quadratic power-like contributions to its radiative corrections, $\Delta\rho$, are absorbed by the renormaliza-

tion of the new parameters of the model: in this case ρ is not a measure of the custodial symmetry breaking.

Mixing Mixing among scalars is another potential problem: absence of mass mixing of the new heavy scalars with the SM Higgs doublet is therefore required since mixings change the scenario.

Consider a model with two doublets and hypercharge $Y = 1/2$ (THDM). These doublets are first rotated (with an angle β) to the Georgi-Higgs basis and successively a mixing-angle α diagonalizes the mass matrix for the CP-even states, h and H. The couplings of h to SM particles are almost the same of a SM Higgs boson with the same mass (at LO) only if we assume $\sin(\beta - \alpha) = 1$. Therefore, interpreting large deviations in the couplings within a THDM should be done only after relaxing this assumption.

The interplay between integrating out heavy scalars and the SM decoupling limit has been discussed in Ref. [60]. In general, decoupling cannot be obtained in terms of only one large scale and can only be achieved by imposing further assumptions on the couplings. Indeed, there are two sources of deviations with respect to the SM, new couplings and modified couplings due to VEV mixings, heavy fields. In general, it is not simple to identify only one scale for new physics (NP); it is relatively simple in the unbroken phase using weak eigenstates but it becomes more complicated when EW symmetry breaking (EWSB) is taken into account and one works with the mass eigenstates. In the second case, one should also take into account that there are relations among the parameters of the beyond-SM (BSM) model, typically coupling constants can be expressed in terms of VEVs and masses; once the heavy scale has been introduced also these relations should be consistently expanded. Once again, the SM decoupling limit cannot be obtained by making only assumptions about one parameter.

In the top-down approach there is some theory, assumed to be UV-complete or valid on a given high energy scale (e.g. some BSM model), and the aim is to implement a systematic procedure for getting the low-energy theory. A typical example would be the Euler-Heisenberg Lagrangian. Systematic low-energy expansions are able to obtain low-energy footprints of the high energy regime of the theory. In the top-down approach the heavy fields are integrated out of the underlying high-energy theory and the resulting effective action is then expanded in a series of local operator terms. Even in the top-down EFT approach one has to be careful: for both tree-level and one-loop processes, the agreement between the effective Lagrangian and a range of UV-complete models depends critically on the appropriate definition of the matching, see Ref. [61].

Custodial symmetry Finally, let us consider custodial symmetry: it is the set of scalar fields that break EW symmetry by developing a VEV. The problem with more VEVs, or one VEV different from $(T, Y) = (\frac{1}{2}, 1)$ (T is isospin and Y is hypercharge), is partially

related to the rho-parameter which at tree-level is given by

$$\rho_{\rm LO} = \frac{1}{2}\frac{\sum_i \left[c_i \mid {\rm v}_i \mid^2 + r_i\, {\rm u}_i^2\right]}{\sum_i Y_i^2 \mid {\rm v}_i \mid^2} \quad c_i = T_i\,(T_i+1) - Y_i^2 \quad {\rm r}_i = T_i\,(T_i+1) \tag{11}$$

where the sum is over all Higgs fields and ${\rm v}_i({\rm u}_i)$ gives the VEV of a complex (real) Higgs field with hypercharge Y_i and weak-isospin T_i. The experimental limits on $\rho - 1$ are rather stringent. The SM Higgs potential is invariant under $SO(4)$; furthermore, $SO(4) \sim SU(2)_{\rm L} \otimes SU(2)_{\rm R}$ and the Higgs VEV breaks it down to the diagonal subgroup $SU(2)_{\rm V}$. It is an approximate symmetry since the $U(1)_{\rm Y}$ is a subgroup of $SU(2)_{\rm R}$ and only that subgroup is gauged. Furthermore, the Yukawa interactions are only invariant under $SU(2)_{\rm L} \otimes U(1)_{\rm Y}$ and not under $SU(2)_{\rm L} \otimes SU(2)_{\rm R}$ and therefore not under the custodial subgroup. Therefore, if we require a new CP-even scalar, which is also in a custodial representation of the group, the ${\rm W}/{\rm Z}$-bosons can only couple to a singlet or a 5-plet [62].

If $(N_{\rm L}\,, N_{\rm R})$ denotes a representation of $SU(2)_{\rm L} \otimes SU(2)_{\rm R}$ we see that the usual Higgs doublet scalar is a $(2\,, \bar{2})$, while the $(3\,, \bar{3}) = 1 \oplus 3 \oplus 5$ contains the Higgs-Kibble ghosts (the 3), a real triplet (with $Y = 2$) and a complex triplet (with $Y = 0$). The Georgi-Machacek model, Ref. [63] has EWSB from both a $(2\,, \bar{2})$ and a $(3\,, \bar{3})$. Custodial symmetry is a statement on the ρ parameter but translation to SVV couplings requires care: when a single source of EWSB is present, custodial symmetry implies $\frac{g_{{\rm S}^0{\rm WW}}}{g_{{\rm S}^0{\rm ZZ}}} = \frac{M_{\rm W}^2}{M_{\rm Z}^2}$. In general $\frac{g_{\rm SWW}}{g_{\rm SZZ}} = \lambda\,\frac{M_{\rm W}^2}{M_{\rm Z}^2}$, e.g. $\lambda = -1/2$ for a 5-plet (already excluded).

6. Results from Run I

In this Section we discuss results from Run 1, including the measurement of the Higgs mass, constraints on the Higgs width, pole observables and off-shell (tail) observables. The results presented here have been published by ATLAS and CMS, and then combined together in Refs. [25,64,24,21,8].

6.1. The measurement of the mass

The most important parameter of a particle is its mass, although the definition of mass and width for an unstable particle requires particular care and is not unique. Here we discuss on-shell quantities.

In any theory the parameters of the Lagrangian cannot be predicted but have to be related to quantities measured experimentally, the so-called input parameter set (IPS). In the SM, once the Higgs boson mass (the "on-shell" mass) is known, the IPS is complete and all properties of the particle can be computed with high precision.

The mass can be measured with very high precision from the $H \to ZZ$ [b] and $H \to \gamma\gamma$ decays, since muons, electrons and photons are reconstructed with high precision, see Refs. [64,25].

The energy scale, the momentum scale and resolution of muons, electrons and photons are excellent in both the experiments. Well-known particles like the Z, Υ, $J/\psi \to 2l$ are used to calibrate the detectors. The decay $Z \to 4l$ is used to validate the procedure. The systematic uncertainty is of $\pm 0.1\% / \pm 0.3\%$ for the muon/electron momentum scale in CMS, and $\pm 0.3\% / \pm 0.1\%$ for for the muon/electron momentum scale in ATLAS. In CMS the mass measurement is performed with a 3D fit using four-lepton invariant mass m_{4l}, associated per-event mass uncertainty δm_{4l}, kinematic discriminant KD, see Ref. [40].

The invariant mass from the di-photon system is given by:

$$m_{\gamma\gamma} = 2 \times E_{\gamma_1} E_{\gamma_2} (1 - \cos(\theta_{12})), \tag{12}$$

thus not only the energy of the photons has to be measured with high precision, but also their directions. The determination of the primary vertex is thus affecting the precision of θ_{12}. In ATLAS, a likelihood discriminant has been developed combining the information on the axis of the shower from the calorimeter, photon conversion, and track recoil. In CMS two Boosted Decision Tree (BDT) have been developed using all the information of the event and then carefully calibrated and cross-checked with $Z \to e^- e^+$ events.

The photon energy calibration is the dominant systematic in the mass reconstruction. The energy scale is determined using $Z \to e^- e^+$ events, then a correction is applied to account for the $e \to \gamma$ difference and subsequently an extrapolation is performed in order to move from the energy scale of the Z to the energy scale of the H. In summary, the systematic uncertainties in the mass measurement from the $\gamma\gamma$ channel are due to the knowledge of the material in front of the electromagnetic calorimeter, the non-linearity of the calorimeter, the calibration of the detector, and the differences between electron and photons.

In Fig. 8 the summary of Higgs boson mass measurements from the individual analyses of ATLAS and CMS [64,25] and from the combined analysis are presented [21]. The systematic uncertainties (narrower, magenta-shaded bands), the statistical uncertainties (wider, yellow-shaded bands), and total uncertainties (black error bars) are indicated. The (red) vertical line and corresponding (gray) shaded column indicate the central value and the total uncertainty of the combined measurement, respectively. In Fig. 9 the scans of twice the negative log-likelihood ratio $2ln\Lambda(m_H)$ as a function of the Higgs boson mass m_H for the ATLAS and CMS combination of the $H \to \gamma\gamma$ (red), $H \to ZZ \to 4l$ (blue), and combined (black) channels are shown. The dashed curves show the results accounting for statistical uncertainties only, with all nuisance parameters associated with systematic uncertainties fixed to their best-fit values. The 1 and 2 standard deviation intervals are indicated by the intersections of the horizontal lines at 1 and 4, respectively, with the log-likelihood scan curves. In Fig. 10 the systematic uncertainties are shown for the measurement in ATLAS, in CMS, and their combination. The mass of the Higgs boson as measured from the first

[b] With the usual caveats in the interpretation of this decay mode.

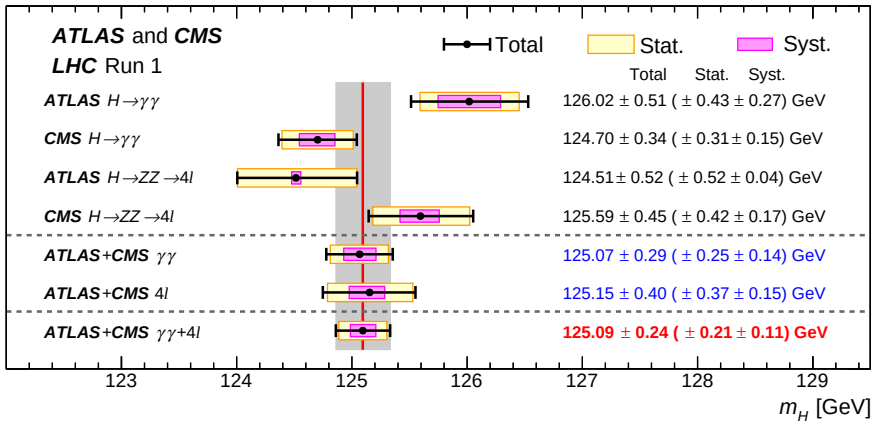

Fig. 8: Summary of Higgs boson mass measurements from the individual analyses of ATLAS and CMS and from the combination. The figure is from Ref. [8].

run at LHC at 7 and 8 TeV center of mass energy is:

$$m_{\rm H} = 125.09 \pm 0.24\ GeV = 125.09 \pm 0.21(stat) \pm 0.11(syst)\ GeV\,, \tag{13}$$

where the total uncertainty is dominated by the statistical term, with the systematic uncertainty dominated by the non linearity of the electromagnetic calorimeter and by the knowledge of the material in front of them and by the lepton energy/momentum scale uncertainty. Compatibility tests are performed to ascertain whether the measurements are consistent with each other, both between the different decay channels and between the two experiments. All tests on the combined results indicate consistency of the different measurements within $1\,\sigma$, while the four Higgs boson mass measurements in the two channels of the two experiments agree within $1.3\,\sigma$.

6.2. On-shell results

The results presented in this section are a selected summary of the combined analysis of the ATLAS and CMS Higgs boson data, as published in Ref. [8]

6.3. The measurement of μ

The signal strengths μ_i^f are defined as the ratios of cross sections and branching fractions to the corresponding SM predictions such that:

$$\mu_i^f = \frac{\sigma_i \cdot BR^f}{(\sigma_i)_{\rm SM} \cdot (BR^f)_{\rm SM}} = \mu_i \times \mu^f\,, \tag{14}$$

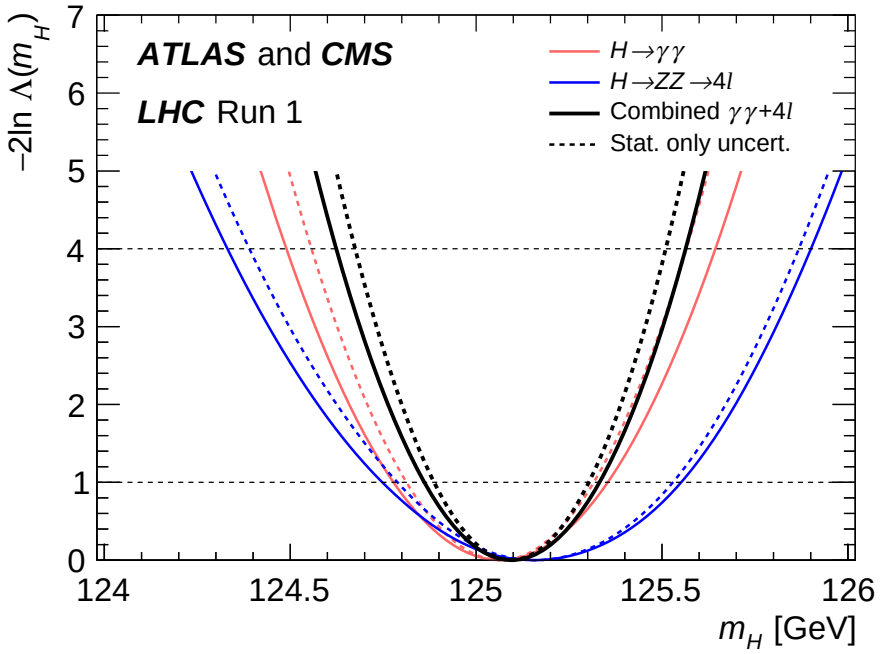

Fig. 9: The scans of twice the negative log-likelihood ratio $2qln\Lambda(m\mathrm{H})$ as a function of the Higgs boson mass m_H for the ATLAS and CMS combination of the $\mathrm{H}\to\gamma\gamma$ (red), $\mathrm{H}\to\mathrm{ZZ}\to 4\mathrm{l}$ (blue), and combined (black) channels. The figure is from Ref. [8]

where the subscript i and superscript f indicate the production mode and decay channel, respectively. By definition all μ_i^f are equal to 1 for the SM Higgs boson.

The simplest and most restrictive signal strength parameterisation is to assume that the μ_i and the μ^f values are the same for all production processes and decay channels. In this case, the SM predictions of signal yields in all categories are scaled by a global signal strength μ. Such a parameterisation, a very special case of the kappa-framework described in Sect. 5, provides the simplest test of the compatibility of the experimental data with the SM predictions.

A fit to the combined ATLAS and CMS data at $E_\mathrm{CM} = 7,8\ TeV$, with μ as the parameter of interest, results in the best-fit value:

$$\mu = 1.09^{+0.11}_{-0.10} = 1.09 \pm 0.07(\mathrm{stat}) \pm 0.04(\mathrm{expt}) \pm 0.03(\mathrm{th\text{-}bkgd})^{+0.07}_{-0.06}(\mathrm{th\text{-}sig}), \qquad (15)$$

where the breakdown of the uncertainties into their four main components is done as described in the following:

- uncertainties, labelled as “stat”, are statistical in nature. These include in particular the statistical uncertainties on background control regions and fit parameters used

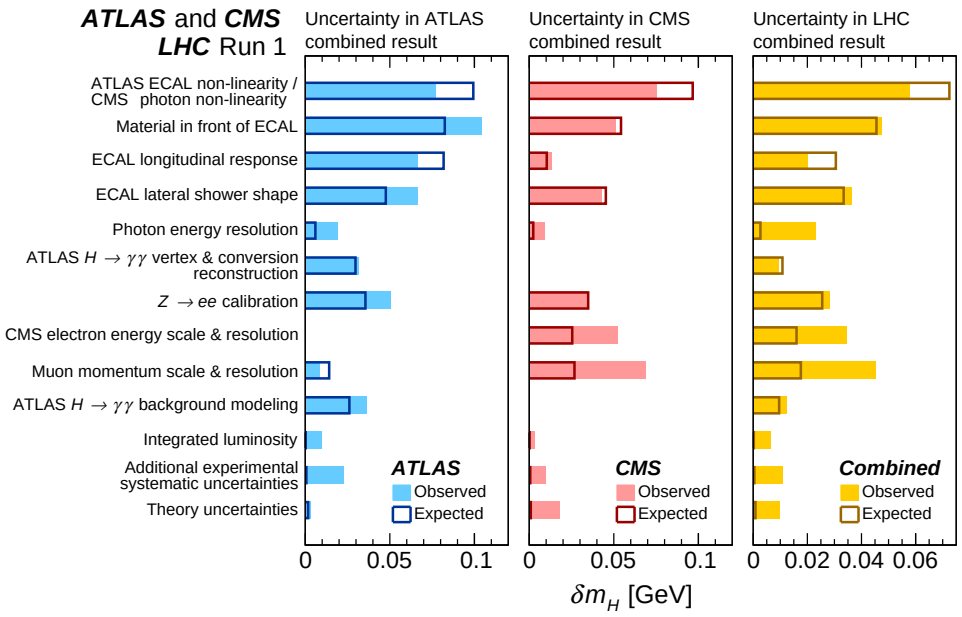

Fig. 10: Systematic uncertainties on the mass for the ATLAS (left), CMS (center), and combined (right). The observed (expected) results are shown by the solid (empty) bars. The figure is from Ref. [8]

to parameterise the backgrounds measured from data;

- theory uncertainties affecting the Higgs boson signal, labelled as "th-sig";
- theory uncertainties affecting background processes only, labelled as "th-bkgd";
- all other experimental uncertainties, labelled as "expt", including those related to the finite size of the MC simulation samples.

The overall systematic uncertainty of $+0.09\,,\,-0.08$ is larger than the statistical uncertainty and its largest component is the theoretical uncertainty on the ggF cross section. This result is consistent with the SM expectation of $\mu = 1$ within less than $1\,\sigma$ and the p-value of the compatibility between the data and the SM prediction is 34%.

As a further step we can measure signal strengths for the different production modes and decays modes. The production processes can be divided into two subgroups: the production via strong interactions as in Fig. 1 (a) and Fig. 3 (a) where the coupling is a fermion coupling, or the production via EW production where the coupling is a vector boson coupling as in Fig. 1 (b) or Fig. 2 (b).

In the experiments, in order to disentangle production mechanisms, activities in the candidates events are analysed:

- the associated production with a Z or a W is identified if high p_{T} leptons, or large missing transverse energy, or low-mass dijets are present and compatible with a electroweak boson in association with a candidate H boson;
- the vector boson production (VBF) is identified if two high p_{T} jets with high invariant mass and large pseudo-rapidity separation are present in the event together with the Higgs candidate.
- the production in association with two top quarks is identified if two top quarks are reconstructed, thus if leptons, large missing transverse energy, multi-jets or b-tagged jets are present in the event and compatible with a top quark decay.
- finally, all the other remaining Higgs candidate events are mostly produced by the gluon-gluon fusion production process.

These differences can be exploited using advanced techniques to enhance the separation between processes, like Boosted Decision Trees.

An interesting result is given by the plot of the signal strength for the “strong production” modes as a function of the signal strength for the "electroweak production" mode, as shown in Fig. 11. Alternatively we can plot the individual signal strengths for each production mode and by decay process: Fig. 12 and Fig. 13. From these figures we can draw the following conclusions:

- the ggF production process is well established,
- there is clear observation of the VBF production mode; the μ value is $5.4\,\sigma$ larger than zero.
- there are indications of the existence of WH and ZH production modes; when combining them together we reach more than $3\,\sigma$ evidence.
- there is not yet sensitivity to the ttH production mode.

Furthermore, we observe that

- the $\mathrm{H} \to \mathrm{ZZ}$, $\mathrm{H} \to \mathrm{WW}$, $\mathrm{H} \to \gamma\gamma$ production modes are well established
- the $\mathrm{H} \to \tau\tau$ decay mode is observed with more than $5\,\sigma$ significance when combining the results of the two experiments.
- there is not yet evidence for the $\mathrm{H} \to \bar{\mathrm{b}}\mathrm{b}$ decay mode.

6.4. The couplings

As a subsequent step we want to disentangle production and decay processes to measure the individual vertices to test the SM and search for new physics. We are not measuring couplings directly, but their ratio with the SM predictions, i.e. the κ parameters as explained in Sect. 5. We will consider the vertices of Fig. 5 and Fig. 6.

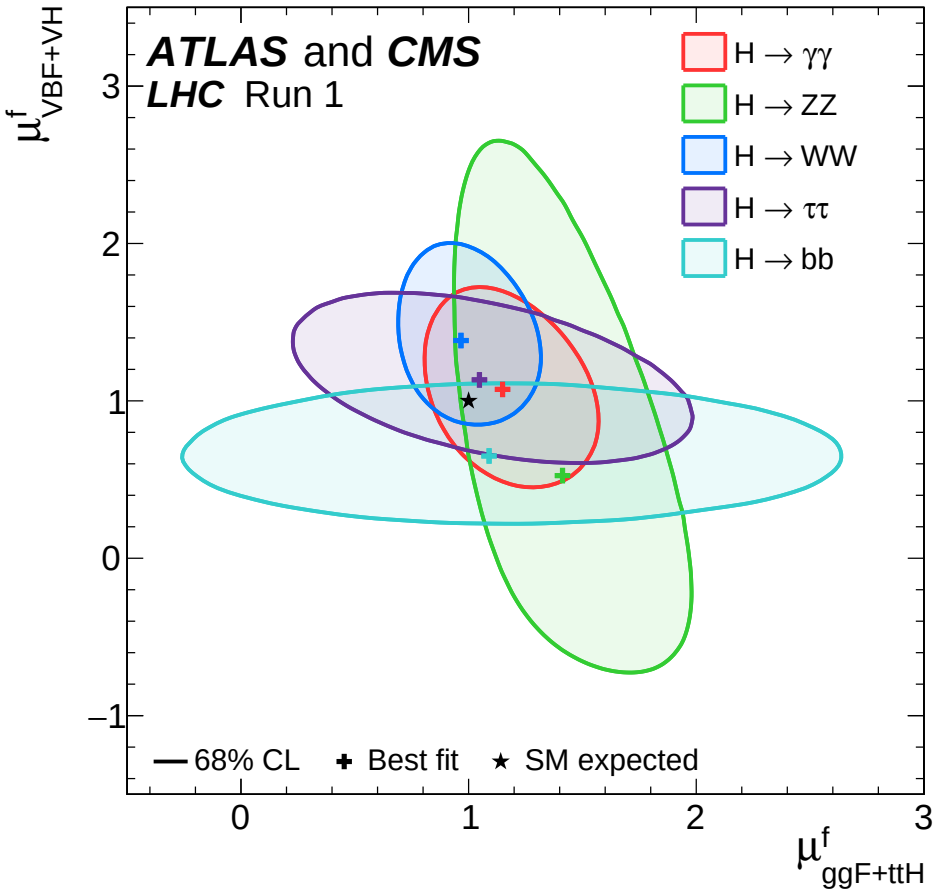

Fig. 11: Negative log-likelihood contours at 68% CL in the $(\mu_{ggF+tt}, \mu_{VBF+VH})$ plane for the combination of ATLAS and CMS, for each of the final state analysed H → ZZ, H → WW, H → γγ, H → ττ, H → bb, and their combination. The SM expectation is also shown as a black star. The figure is from Ref. [8].

Custodial Symmetry in the kappa framework As explained in Sect. 5 one of the first important tests of the SM is to validate the Custodial Symmetry. The parameter

$$\rho = M_W^2/M_Z^2 \cdot cos^2\theta_W \tag{16}$$

is 1 at tree level. At LEP the experiments have measured: $\rho = 1.005 \pm 0.001$, i.e. 5 sigma away from 1, but in perfect agreement with the theoretical value of $\rho = 1 + \Delta\rho$ when radiative corrections are correctly taken into account. Measuring the W to Z coupling ratio from H decays, means deriving the ratio between boson masses, thus ρ; it will tell us if the object produced is a (minimal) SM-Higgs boson like. In the κ framework we measure $\lambda_{WZ} = \kappa_W/\kappa_Z$ that is expected to be 1 in the SM. The result is shown in Fig. 14 and it is

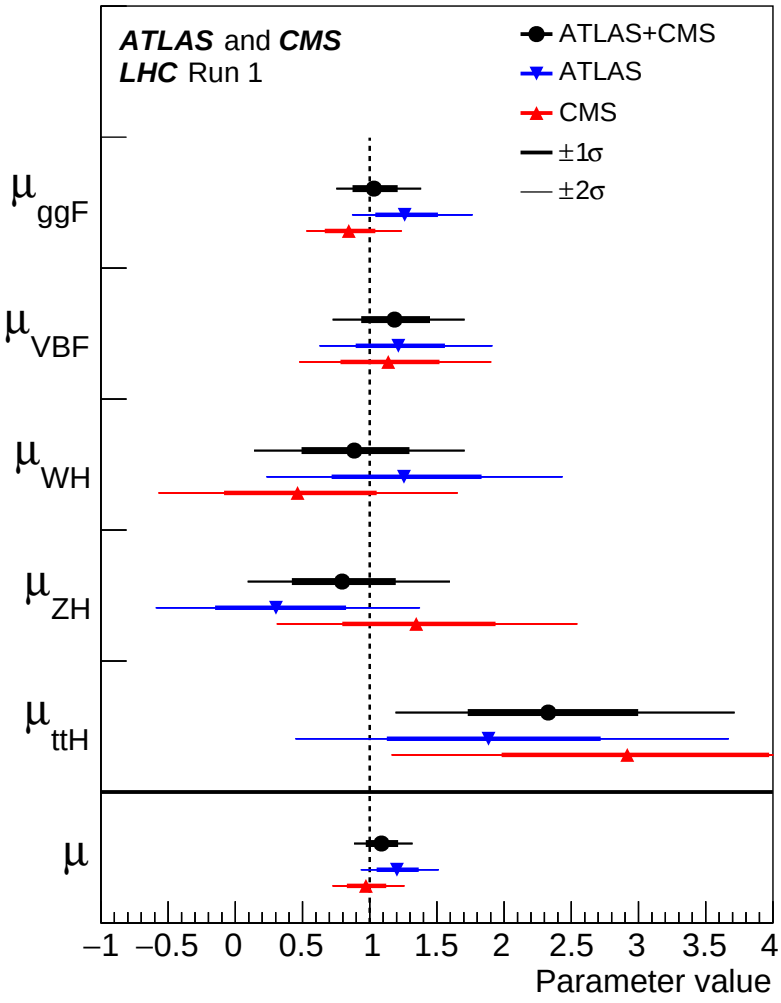

Fig. 12: Best fit results for the production signal strengths for the combination of ATLAS and CMS data. Also shown are the results from each experiment. The error bars indicate the $1\,\sigma$ (thick lines) and $2\,\sigma$ (thin lines) intervals. The measurements of the global signal strength μ are also shown. The figure is from Ref. [8].

$\lambda_{WZ} = 0.89^{+0.10}_{-0.09}$, i.e. consistent with one within $1\,\sigma$. Thus we can, from now on, assume $\kappa_W = \kappa_Z$.

Vector and fermion Higgs couplings in the kappa framework. The further step is to assume that all fermion couplings scale as κ_f while all vector boson couplings scale as κ_V. The result is shown in Fig. 15. The figures shows the 5 different final states and their combination. The shapes of the various contours can be easily understood by writing the

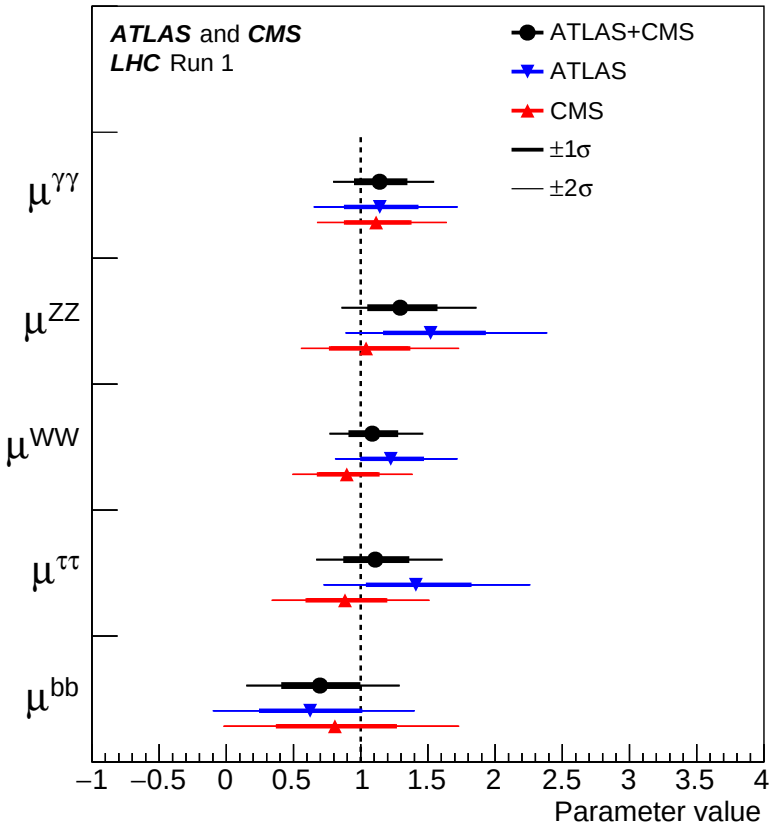

Fig. 13: Best fit results for the decay signal strengths for the combination of ATLAS and CMS data. Also shown are the results from each experiment. The error bars indicate the $1\,\sigma$ (thick lines) and $2\,\sigma$ (thin lines) intervals. The figure is from Ref. [8].

cross-section formula as a function of κ_f and κ_V.

$$(\sigma \times BR)_{(ii\to \mathrm{H},\mathrm{H}\to jj)} = \sigma_{ii} \times \Gamma_{jj}/\Gamma_\mathrm{H} = \sigma_{SM}(ii \to \mathrm{H}) \times BR(\mathrm{H} \to jj) \times \kappa_i \cdot \kappa_j/\kappa_\mathrm{H} \quad (17)$$

In the denominator we have the width of the Higgs, that for a Higgs of 125 *GeV* is dominated by the $\bar{\mathrm{b}}\mathrm{b}$ decay channel, i.e. by κ_f. If the production mode is ggF then the initial state is contributing with κ_f, while if the production is via VBF or VH, in the equation there will be a κ_V in the numerator. As an example: the HZZ channel is dominated by the ggF production mode, thus it will behave as $\kappa_f\kappa_V/\kappa_f$, thus it will depend on κ_V. In $\mathrm{H} \to \gamma\gamma$ the H boson does not couple directly to the photon, but via the diagrams of Fig. 6; it will behave as $\kappa_i \times (8.6\kappa_V - 1.8\kappa_f)/\kappa_f$, where $i = \mathrm{f}$ for ggF and $i = \mathrm{V}$ for VBF. Thus the behaviour of the red region in the plot.

Model with 9 parameters. As a subsequent step, the individual couplings, actually the strength modifier κ for each of the couplings, can be extracted. The rate of the Higgs boson

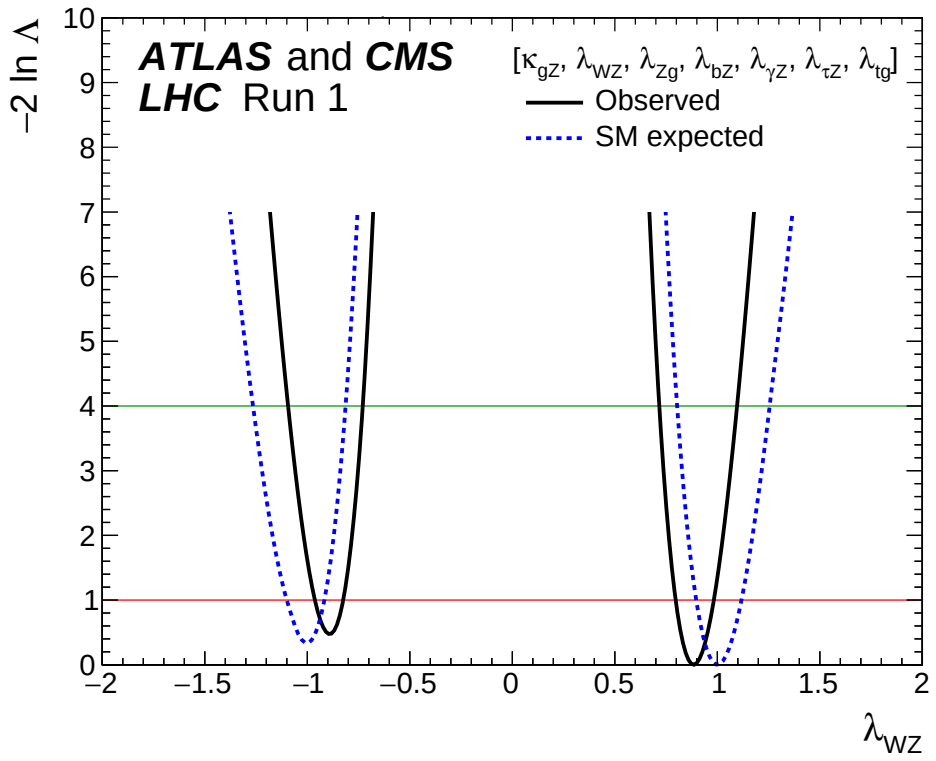

Fig. 14: Observed (solid line) and expected (dashed line) negative log-likelihood scans for λ_{WZ}. All the other parameters of interest from the list in the legend are also varied in the minimisation procedure. The red (green) horizontal lines at the $-2ln\Lambda$ value of 1 (4) indicate the value of the profile likelihood ratio corresponding to a $1\,\sigma$ ($2\,\sigma$) CL interval. The figure is from Ref. [8].

production is inversely proportional to the Higgs boson width, which is sensitive to invisible or undetected Higgs boson decays predicted by many BSM theories. To directly measure the individual coupling modifiers, an assumption on the Higgs boson width is necessary. Two scenarios are considered: the first one assumes that the Higgs boson does not have any BSM decays, $BR_{BSM} = 0$, while the second one leaves BR_{BSM} free, but assumes $\kappa_W \leq 1$, $\kappa_Z \leq 1$ (i.e. $\kappa_V \leq 1$) and $BR_{BSM} \geq 0$. Notice that these latter constraints are compatible with a wide range of BSM physics models. BSM physics can also contribute in the loop-induced processes for the gg $\rightarrow$ H production and and H $\rightarrow \gamma\gamma$ decay. A dedicated measurement of these two processes will also be presented. BSM physics will also appear as a deviation from 1 of the individual coupling modifiers κ_i. The parameters of interest of the fits to the data are thus the seven independent coupling modifiers: γ, g, Z, W, b, t, and τ, i.e. one for each SM particle involved in the production processes and decay channels studied, plus $BR_{\rm BSM}$ in the case of the second fit.

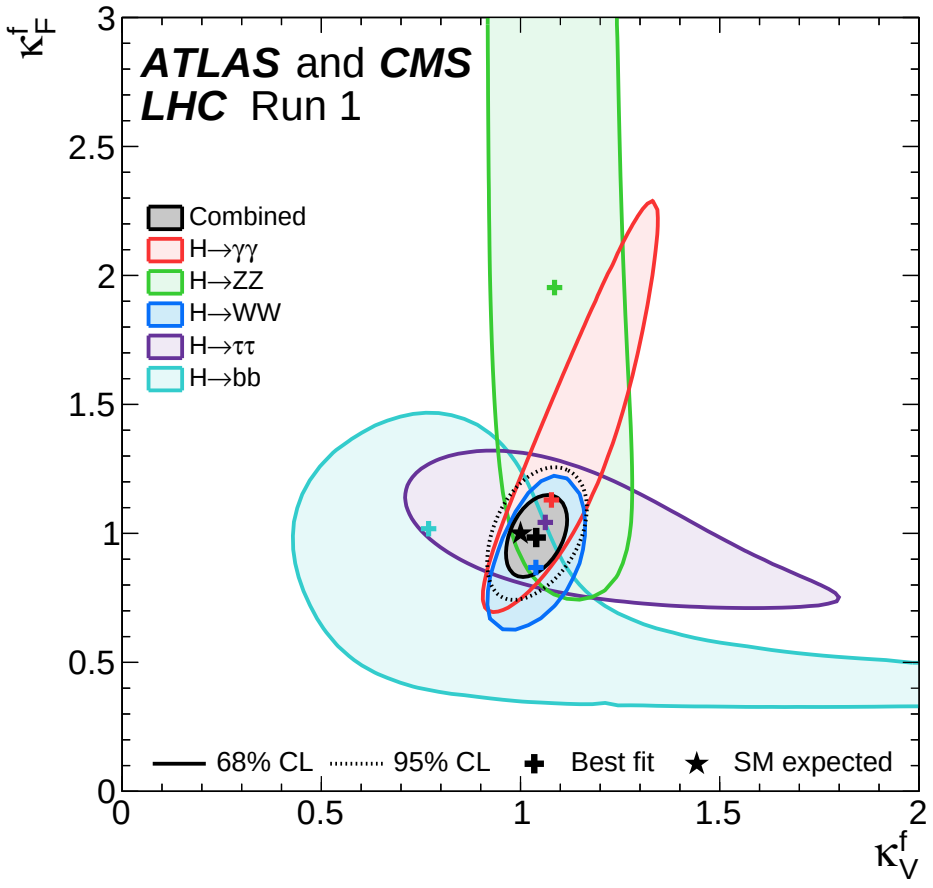

Fig. 15: Negative log-likelihood contours at 68% CL in the (κ_f, κ_V) plane for the combination of ATLAS and CMS and for the individual decay channels as well as for their global combination, assuming that all coupling modifiers are positive. The figure is from Ref. [8].

In Fig. 16, the fit results for the two parameterisations: the first one for $BR_{BSM} \geq 0$ and $\kappa_V \leq 1$, and the second one for $BR_{BSM} = 0$. The measured results for the combination of ATLAS and CMS are reported together with their uncertainties, as well as the individual results from each experiment. The error bars indicate the $1\,\sigma$ and $2\,\sigma$ (thin lines) intervals.

The gluon and photon loops. A scenario were new heavy particles contribute to loop-induced processes in Higgs boson production or decay, and all the couplings to SM particles are the same as in the SM, and thus $BR_{BSM} = 0$, could be tested. In this case only the gluon-gluon production and decay loops in the $H \to \gamma\gamma$ could be affected by the presence of additional particles. The results of this fit, in which only the effective coupling modifiers κ_γ and κ_g are the free parameters, and with all the other coupling modifiers fixed to their

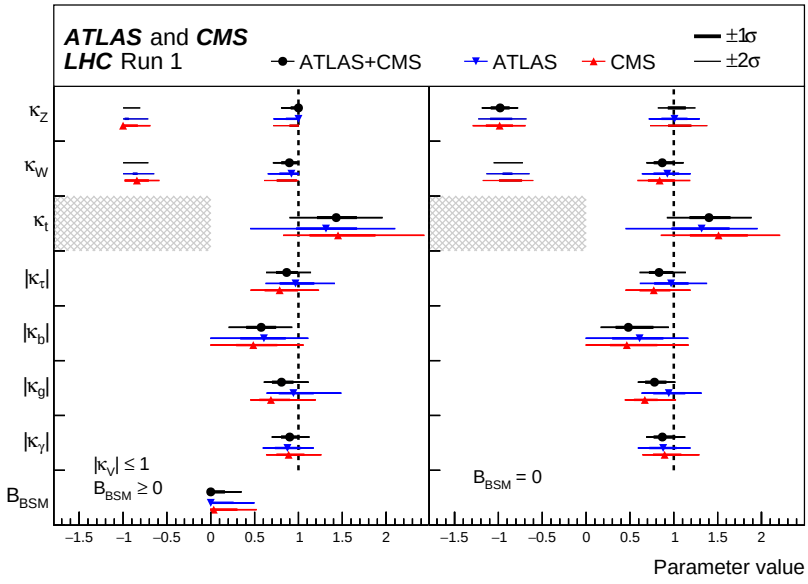

Fig. 16: The fit results for two parameterisations: the first one for $BR_{BSM} \geq 0$ and $\kappa_V \leq 1$, and the second one for $BR_{BSM} = 0$. The measured results for the combination of ATLAS and CMS are reported together with their uncertainties, as well as the individual results from each experiment. The error bars indicate the $1\,\sigma$ and $2\,\sigma$ (thin lines) intervals. The hatched areas show the non-allowed regions for the κ_t parameter, which is assumed to be positive without loss of generality. The figure is from Ref. [8].

SM value of unity, is shown in Fig. 17. The point (κ_γ= 1,κ_g=1) lies within the 68% CL contour and the p-value of the compatibility between the data and the SM predictions is 82%.

Model with 6 parameters. Given that the effective coupling modifiers κ_g and κ_γ are measured to be consistent with the SM expectations, we assume in the following that there are no new particles in these loops. The SM relations for the loops are used with their respective coupling modifiers. This leads to a parameterisation with six free coupling modifiers: W, Z, t, b, τ and μ. The results of the $H \to \mu\mu$ analysis are included for this specific case. In this more constrained fit, it is also assumed that $BR_{BSM} = 0$. Fig. 18 shows the results of the fit for the combination of ATLAS and CMS and separately for each experiment. From the comparison of these results with those of the fitted decay signal strengths of Fig. 13 it is evident that the 6 parameters fit results in lower values of the coupling modifiers than the SM expectation. This is a consequence of the low value of κ_b, as measured by the experiments. A low value of κ_b reduces the total Higgs boson width through the dominant $H \to bb$ partial decay width, and, as a consequence, the measured values of all the coupling modifiers are reduced.

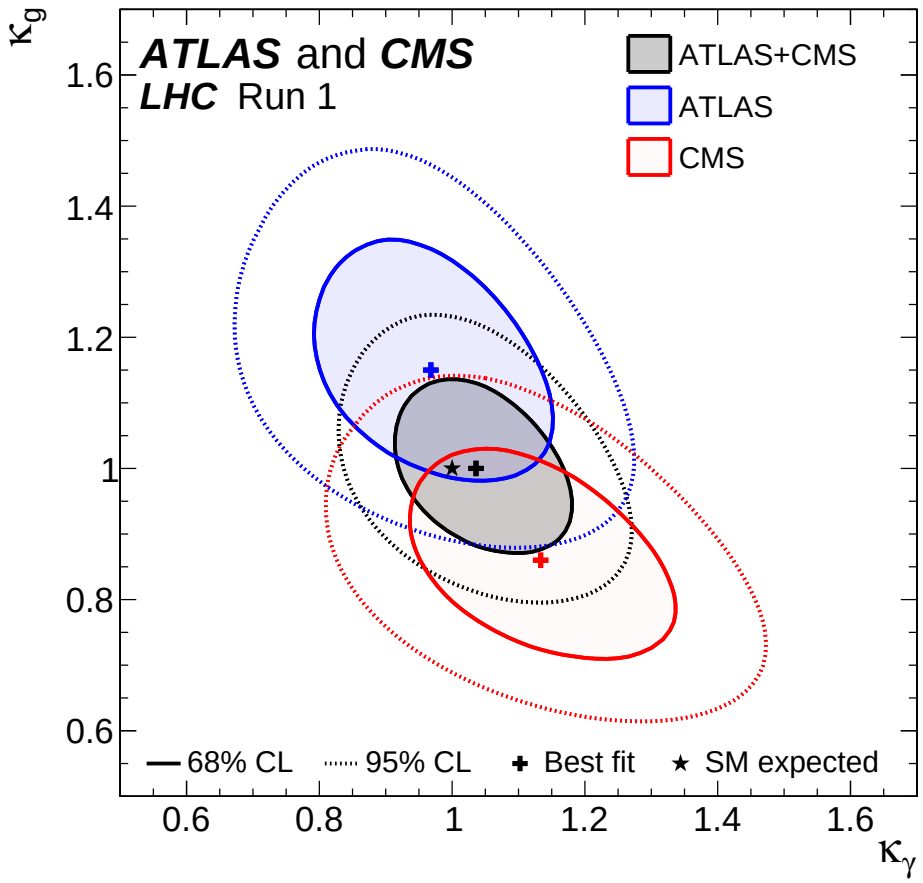

Fig. 17: Negative log-likelihood contours at 68% and 95% CL in the (κ_γ,κ_g) plane for the combination of ATLAS and CMS and for each experiment separately, as obtained from the fit to the parameterisation constraining all the other coupling modifiers to their SM values and assuming $BR_{BSM} = 0$. The figure is from Ref. [8].

Lepton vs quark, up-fermion vs down-fermion. Models of new physics beyond the SM (as the THDM or MSSM) predict differences in the coupling modifications for up-type fermions versus down-type fermions or for leptons versus quarks. The parameter of interest are $\lambda_{du} = \kappa_d/\kappa_u$, for the up- and down-type fermion symmetry test, and $\lambda_{lq} = \kappa_l/\kappa_q$ for the lepton and quark symmetry test.

The combined experimental result for the up and down quark symmetry test is: $\lambda_{du} = 0.91^{+0.12}_{-0.11}$, where the down-type fermion couplings are mainly probed by the $H \to bb$ and $H \to \tau\tau$ decays.

The combined experimental result for the lepton and quark symmetry test is: $\lambda_{lq} =$

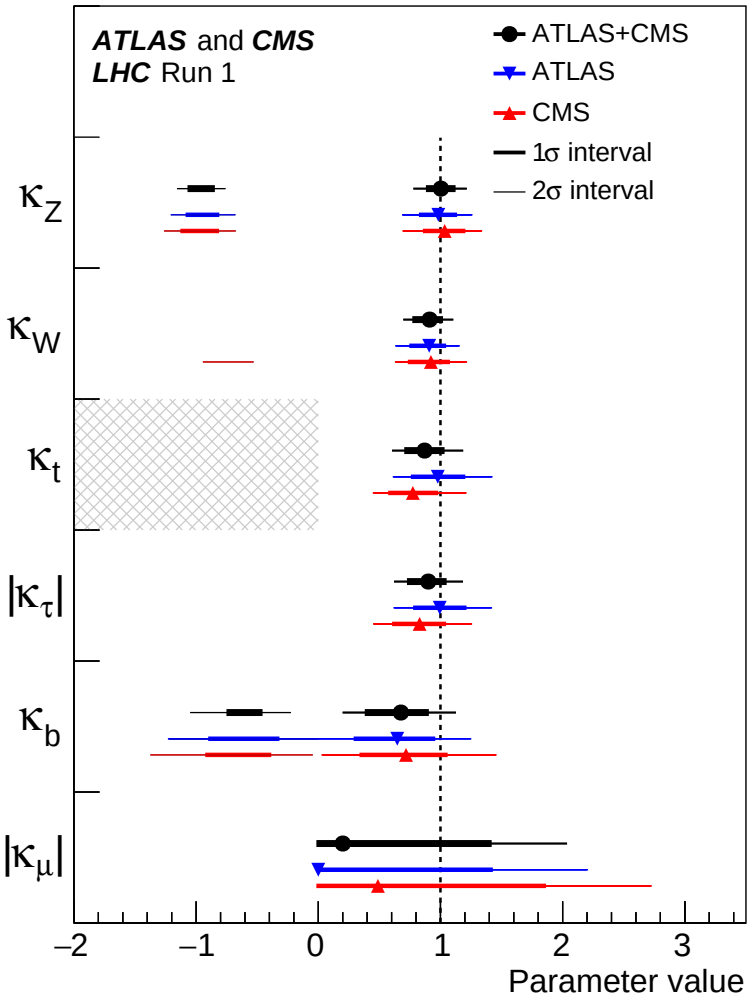

Fig. 18: Best fit values of parameters for the combination of ATLAS and CMS , and separately for each experiment, for the parameterisation assuming the absence of BSM particles in the loops. The hatched area indicates the non-allowed region for the parameter that is assumed to be positive without loss of generality. The error bars indicate the $1\,\sigma$ (thick lines) and $2\,\sigma$ (thin lines) intervals. For the parameters with no sensitivity to the sign, only the absolute values are shown. The figure is from Ref. [8].

$1.06^{+0.15}_{-0.14}$, where the quark couplings are mainly probed by the ggF process, the $\mathrm{H} \to \gamma\gamma$ and $\mathrm{H} \to \mathrm{bb}$ decays, and to a lesser extent by the ttH process; while the lepton couplings are probed by the $\mathrm{H} \to \tau\tau$ decays. The results are expected to be insensitive to the relative sign of the couplings because there is no sizeable lepton-quark interference in any of the relevant Higgs boson production and decay processes.

6.5. Ratios of cross sections and branching ratios

The measured Higgs boson rates are sensitive to the product of the cross sections times the branching ratios. Thus, from the measurements of the rate of a single process, the cross sections and decay branching ratios cannot be separately determined in a model-independent way. Using more processes, ratios of cross sections and branching ratios can be extracted, from a combined fit to the data. This could be achieved by normalising the yield of any specific channel $i \to \mathrm{H} \to \mathrm{f}$ to the reference process $\mathrm{gg} \to \mathrm{H} \to \mathrm{ZZ}$. This channel has been chosen by the experiments because the combined value for $\sigma(\mathrm{gg} \to \mathrm{H} \to \mathrm{ZZ})$ has the smallest systematic and one of the smallest overall uncertainties.

Expressing the measurements through ratios of cross sections and branching ratios has the advantage that the ratios are independent of the theoretical predictions on the inclusive production cross sections and decay branching ratios of the Higgs boson. In particular, they are not subject to the dominant signal theoretical uncertainties on the inclusive cross sections for the various production processes. The remaining theoretical uncertainties are the ones due to the acceptances and selection efficiencies in the various categories, for which SM Higgs boson production and decay kinematics are assumed in the simulations.

The product of the cross section and the branching ratio of $i \to \mathrm{H} \to \mathrm{f}$ can then be expressed using the ratios as:

$$\sigma_i \cdot BR^{\mathrm{f}} = \sigma(\mathrm{gg} \to \mathrm{H} \to \mathrm{ZZ}) \times \left(\frac{\sigma_i}{\sigma_{ggF}}\right) \times \left(\frac{BR^{\mathrm{f}}}{BR^{\mathrm{ZZ}}}\right), \tag{18}$$

where $\sigma(\mathrm{gg} \to \mathrm{H} \to \mathrm{ZZ}) = \sigma_{ggF} \cdot BR^{\mathrm{ZZ}}$ and the narrow width approximation is assumed. Since the cross section $\sigma(\mathrm{gg} \to \mathrm{H} \to \mathrm{ZZ})$ is constraining the normalisation, the ratios in Eq. 18 can be determined separately, based on the five production processes (ggF, VBF, WH, ZH, and ttH) and five decay modes (HZZ, HWW, Hγγ, Htt, and Hbb). The combined fit results is presented as a function of nine parameters of interest: the reference cross section times branching ratio, $\sigma(gg \to \mathrm{H} \to \mathrm{ZZ})$, four ratios of production cross sections, σ_i/σ_{ggF}, and four ratios of branching ratios, $BR^{\mathrm{f}}/BR^{\mathrm{ZZ}}$, as shown in Fig. 19. In this figure the fit results are normalised to the SM predictions for the various parameters and the shaded bands indicate the theory uncertainties on these predictions. The theory uncertainties on the ratios of branching ratios are very small, and therefore almost not visible. The combination of 7 and 8 TeV data is carried out under the assumption that the ratios of the production cross sections with respect to the SM predictions are the same at $\sqrt{s} = 7$ and 8 TeV.

The total relative uncertainty on $\sigma(\mathrm{gg} \to \mathrm{H} \to \mathrm{ZZ})$ is approximately 19%, where the dominant contribution is the statistical one. The total relative systematic uncertainty is $\sim 4\%$. The ratio of cross sections $\sigma_{VBF}/\sigma_{ggF}$ and the ratios $BR^{\mathrm{WW}}/BR^{\mathrm{ZZ}}$ and $BR^{\gamma\gamma}/BR^{\mathrm{ZZ}}$ are measured with a relative uncertainty of approximately 30%, while the $BR^{\tau\tau}/BR^{\mathrm{ZZ}}$ ratio is measured with a relative accuracy of approximately 40%.

The p-value of the compatibility between the data and the SM predictions is 16%. The

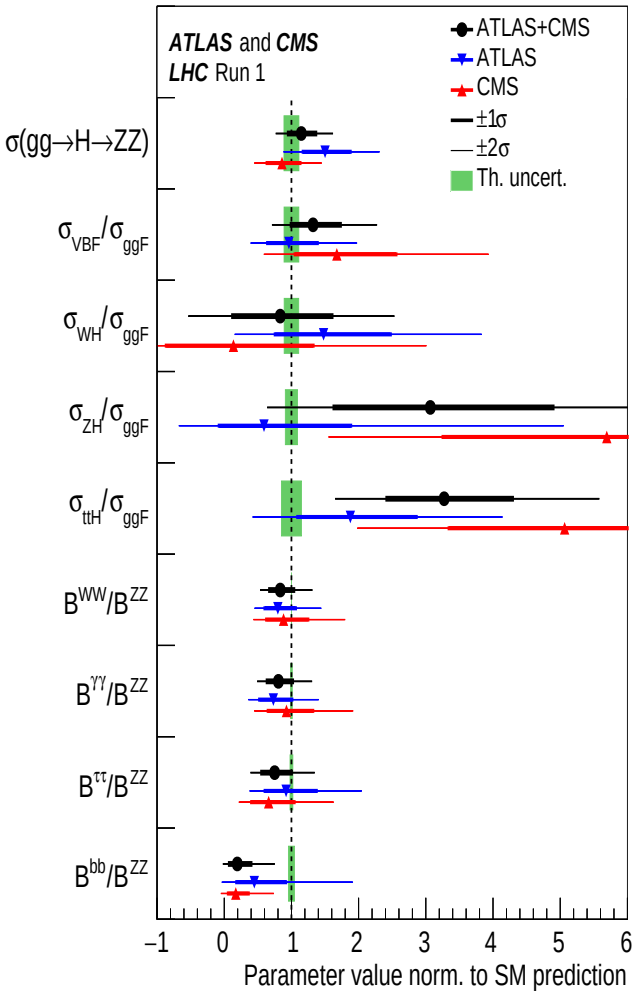

Fig. 19: Best-fit values of the $\sigma(\mathrm{gg} \to \mathrm{H} \to \mathrm{ZZ})$ cross section and of ratios of cross sections and branching ratios, as obtained from the generic parameterisation described in the text for the combination of ATLAS and CMS measurements and for each experiment individually. The error bars indicate the 1σ (thick lines) and 2σ (thin lines) intervals. In this figure, the fit results are normalised to the SM predictions for the various parameters and the shaded bands indicate the theory uncertainties on these predictions. The figure is from Ref. [8].

most precise measurements are all consistent with the SM predictions within less than 2σ. The production cross-section ratio $\sigma_{\mathrm{ttH}}/\sigma_{ggF}$ relative to the SM ratio, is measured to be $3.3^{+1.0}_{-0.9}$, corresponding to an excess compared to the SM prediction of approximately 2.3σ. This excess is mainly due to the multi-lepton categories. The ratio of branching ratios $BR^{\mathrm{bb}}/BR^{\mathrm{ZZ}}$ relative to the SM ratio is measured to be $0.19^{+0.21}_{-0.12}$. In this parameterisation,

the high values found for the production cross-section ratios for the ZH and ttH processes induce a low value for the Hbb decay branching ratio because the Hbb decay channel does not contribute to the observed excesses. The result is an overall deficit compared to the SM prediction of approximately $2.5\,\sigma$.

6.6. A summary plot

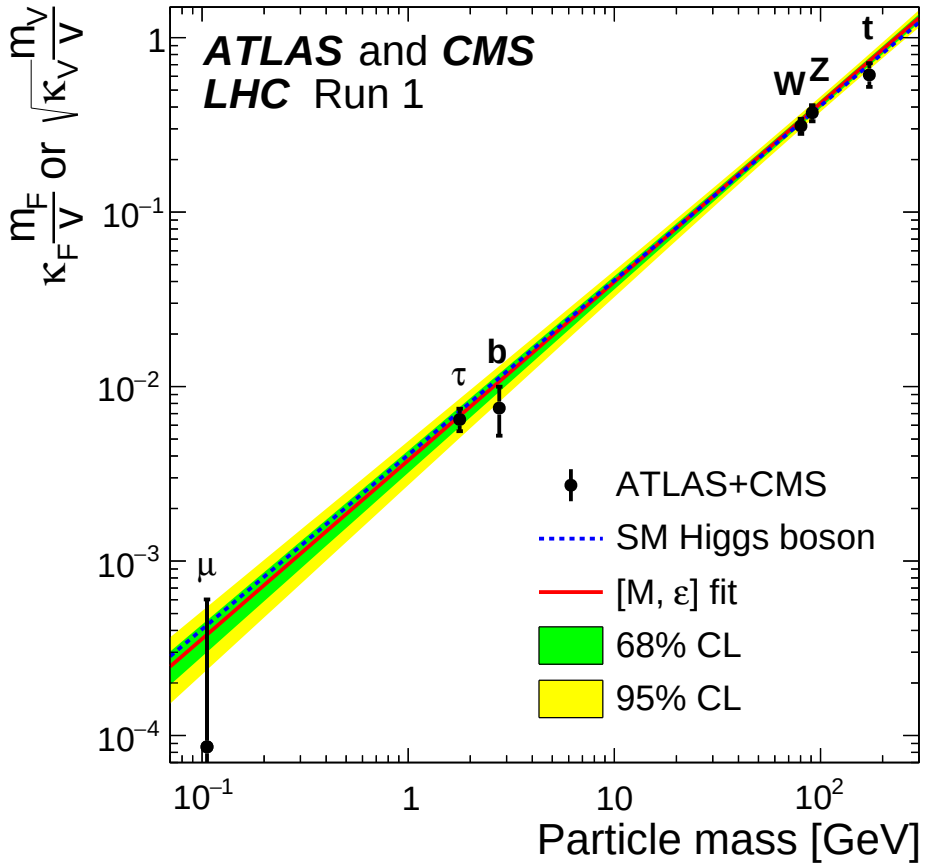

Fig. 20: Fit results as a function of the particle mass in the case of the parameterisation with reduced coupling modifiers $y_{V,i}$ for the weak vector bosons, and $y_{f,i}$ for the fermions, as explained in the text, for the combination of ATLAS and CMS. The dashed line indicates the predicted dependence on the particle mass for the SM Higgs boson. The solid (red) line indicates the best fit result to the [M,ε] phenomenological model of Ref. [65] with the corresponding 68% and 95% CL bands in green and yellow. The figure is from Ref. [8].

The relation between the coupling modifiers and the SM predictions can be presented as a

function of the mass of the particles to which the H boson is coupling. The coupling of the Higgs to vector bosons of mass m_{V} when expressed as a function on κ_{V} is:

$$y_{V,i} = \sqrt{\kappa_{\mathrm{V},i}\frac{g_{\mathrm{V},i}}{2v}} = \sqrt{\kappa_{\mathrm{V},i}}\frac{m_{\mathrm{V},i}}{v} \tag{19}$$

where $g_{\mathrm{V},i}$ is the absolute Higgs boson coupling strength and $v = 246\ GeV$ is the vacuum expectation value of the Higgs field.

The coupling of the Higgs to the fermions of mass m_{f} when express as a function on κ_{f} is:

$$y_{f,i} = \kappa_{\mathrm{f},i}\frac{g_{\mathrm{f},i}}{\sqrt{2}} = \kappa_{\mathrm{f},i}\frac{m_{\mathrm{f},i}}{v}. \tag{20}$$

The linear scaling of the reduced coupling modifiers as a function of the particle masses is shown in Fig. 20 and indicates the consistency of the measurements with the SM.

6.7. Theoretical perspectives

In the previous Section different variants of the original kappa-framework have been presented and discussed in relation to experimental data. Here we briefly summarise theoretical perspectives on improving the experimental strategy.

One possibility to go beyond the kappa framework is represented by the SM effective field theory: SMEFT will be described in details in Section 7 and it is based on the Lagrangian of Eq.(44), which is the SM Lagrangian with the addition of dim = 6 operators.

Several (theoretical) analyses have been performed with the available Run 1 data, as summarised in Ref. [66], see also Refs. [67,68,69]. These analyses always use a subset of the full set of dim = 6, gauge invariant operators (e.g. the so-called "Warsaw" basis) and show a good agreement, with differences due to different sets of assumptions. The results can be summarised by saying that current measurements show good agreement with the SM hypothesis. In practice, the predicted number of events for a given final state F is obtained as

$$\mathrm{N_{th}} = \sigma\left(\mathrm{H}+\mathrm{X}\right) \times \mathrm{BR}\left(\mathrm{H} \to \mathrm{YY}\right) \times \mathrm{BR}\left(\mathrm{X},\mathrm{Y} \to \mathrm{F}\right) \times \mathscr{L}\,. \tag{21}$$

The "number of events" is

$$\mathrm{N_{ev}} = \mathrm{N_{th}}\,\varepsilon_p\,\varepsilon_d\,, \tag{22}$$

where $\varepsilon_{p,d}$ are the efficiencies to measure production and decay and $\mathscr{L}$ is the luminosity. Theoretical uncertainties for production and decay channels are shown in Tab. 4 while the order of available calculations is given in Tab. 2. In Tab. 4 (differently from Tab. 2 as used by the experimental analyses) the uncertainty is given by the linear sum of the QCD scale variation and of the PDF uncertainty as presented in Refs. [9,10]. Extrapolating to

Table 4: Theoretical uncertainties for production and decay channels in %

Production	Decay		
$pp \to H$	14.7	$H \to \bar{b}b$	6.1
$pp \to H+j$	15	$H \to \gamma\gamma$	5.4
$pp \to H+2j$	15	$H \to \tau^+\tau^-$	2.8
$pp \to HZ$	5.1	$H \to 4l$	4.8
$pp \to HW$	3.7	$H \to 2l2\nu$	4.8
$pp \to \bar{t}tH$	12	$H \to Z\gamma$	9.4
		$H \to \mu^+\mu^-$	2.8

13 *TeV* a major improvement is expected, in particular when differential distributions will be included.

Global constraints of the SMEFT have been developed in Ref. [70], with results that show how the SMEFT theory uncertainties should not be neglected in future fits, see also Ref. [71]. Preliminary results of a Bayesian fit to the Wilson coefficients using data on EW precision observables and Higgs boson signal strengths have been presented in Ref. [72].

Ref. [73] deals with Higgs production through weak boson fusion with subsequent decay to bottom quarks. By combining jet substructure techniques and matrix element methods in different limits the authors motivate this channel as a probe of the bottom-Yukawa interactions in the boosted regime.

The possibility to separate, in gluon fusion, loop-induced Higgs boson production from point-like production has been examined in Ref. [74]. The Higgs boson is reconstructed in the $H\gamma\gamma$ final state at very large transverse momentum. Using the Higgs boson yields (normalised to the overall rate) and the shape of the Higgs boson p_T distribution, the two hypotheses can be separated with 2 standard deviations with an integrated luminosity of about 500 fb^{-1}. The largest experimental uncertainty affecting this estimate is the background event yield. The theoretical uncertainties from missing top mass effects are large, but can be decreased with dedicated calculations.

For the measured Higgs boson mass of 125 *GeV* the limit of heavy top quarks provides a reliable approximation as long as the relative QCD corrections are scaled with the full mass-dependent LO cross section. In this limit the Higgs coupling to gluons can be described by an effective Lagrangian. The same approach has been applied to the coupling of more than one Higgs boson to gluons [75], deriving the effective Lagrangian for multi-Higgs couplings to gluons up to N^4LO thus extending previous results for more than one Higgs boson.

The authors of Ref. [76] have examined the constraints on the trilinear Higgs coupling that originate from associated and vector boson fusion Higgs production in the context of the SMEFT, showing that future LHC runs may be able to probe modifications of the coupling with a sensitivity similar to the one that is expected to arise from determinations of double-

Higgs production.

The authors of Ref. [77] have proposed a method to determine the trilinear Higgs self coupling that is alternative to the direct measurement of Higgs pair production total cross sections and differential distributions. The method relies on the effects that electroweak loops featuring an anomalous trilinear coupling would imprint on single Higgs production at the LHC. It is found that the bounds on the self coupling are already competitive with those from Higgs pair production and will be further improved in the current and next LHC runs.

The authors of Ref. [78] have proposed a novel strategy to constrain the bottom and charm Yukawa couplings by exploiting LHC measurements of transverse momentum distributions in Higgs production. The method does not rely on the reconstruction of exclusive final states or heavy-flavour tagging. Compared to other proposals it leads to an enhanced sensitivity to the Yukawa couplings due to distortions of the differential Higgs spectra from emissions which either probe quark loops or are associated to quark-initiated production.

The authors of Ref. [79] investigated anomalous interactions of the Higgs boson with heavy fermions, employing shapes of kinematic distributions, presenting applications of event generation, reweighting techniques for fast simulation of anomalous couplings, as well as matrix element techniques for optimal sensitivity.

The authors of Ref. [80] have studied Higgs boson production in association with a top quark and a W boson at the LHC. At NLO in QCD, tWH interferes with $\bar{\mathrm{t}}\mathrm{t}\mathrm{H}$ and a procedure to meaningfully separate the two processes needs to be developed.

The authors of Ref. [81] analysed the production of a top quark pair through a heavy scalar at the LHC. While the background and the signal can be obtained at NNLO and NLO in QCD respectively, that is not the case for their interference, which is currently only approximately known at NLO. In order to improve the accuracy of the prediction for the interference term, the effects of extra QCD radiation are considered: as a result, it is found that the contribution of the interference is important both at the total cross-section level and, most importantly, for the line-shape of the heavy scalar.

The main lesson from Run 1 of LHC is that, to first approximation, we have a (minimal) SM-like scalar sector. To be more precise, the best precisions achieved are approximately 30% for the ratio of cross sections VBF/ggF (vector boson fusion and gluon-gluon fusion) and for the ratios of branching fractions, $\mathrm{BR}(\mathrm{WW})/\mathrm{BR}(\mathrm{ZZ})$ and $\mathrm{BR}(\gamma\gamma)/\mathrm{BR}(\mathrm{ZZ})$. The ratios of coupling modifiers (kappa parameters) are measured with precisions of approximately $10 \rightarrow 20\%$. The main message from Run 1: it is important to check the apparent minimality of the Higgs sector as it is important to anticipate deviations. The improvements expected from Run 2 will come from greater statistics, greater kinematic range and improvement in theoretical uncertainties. To be considered together with the LHC data, are the EW precision data (EWPD). For instance, measurements of the W mass provide an important consistency check of the SM and constrain the possibility of physics beyond the SM.

The work of Ref. [82] has shown that the extra error introduced in these measurements due to SMEFT higher dimensional operators is subdominant to the current experimental systematic errors. This means that the leading challenge to interpreting these measurements in the SMEFT is the pure theoretical uncertainty in how these measurements are mapped to Lagrangian parameters.

Inclusion of EWPD in a global fit deserves additional comments. Usually bounds on the coefficients are obtained in two ways: individual coefficients are switched one at a time, or marginalised in a simultaneous fit. In Ref. [71] the global constraint picture on SMEFT parameters has been updated with the conclusion that stronger constraints can be obtained by using some combinations of Wilson coefficients, when making assumptions on the UV completion of the SM. To summarise: global fits show that the degree of constraint on the SMEFT parameters is strongly dependent on the assumptions made about possible UV physics matched onto the SMEFT. The theoretical uncertainty, due to neglected terms in the SMEFT, is also UV dependent.

It is worth noting that fitting dim = 6 Wilson coefficients to LHC Higgs data can be done and has been done for Run 1 data, but not by members of the ATLAS and CMS collaborations. What has been learnt is that kinematic distributions can significantly improve the multi-dimensional parameter by resolving strong correlations present in total rate measurements.

As discussed in Refs. [83,84], a few selected kinematic distributions can be used to collect information on modified Higgs couplings, for example in the gluon fusion production process. In the top-gluon-Higgs sector one can compare three different analysis strategies: a modified p_{T} spectrum of boosted Higgs production in gluon fusion [85], off-shell Higgs production, and a measurement of the gluon fusion vs $\bar{\mathrm{t}}\mathrm{t}\mathrm{H}$ production rates. Unfortunately, explicit threshold effects in boosted Higgs production are too small to be observable in the near future [86]. Global analyses including kinematic information in all Higgs channels cannot rely on the kappa framework, but they could be based on a SMEFT. Such analyses provide potentialities and challenges at the same time [83,84].

6.8. Off-shell results, experimental constraints on the width

In Ref. [87] the off-shell production cross section has been shown to be sizeable at high ZZ-invariant mass in the gluon fusion production mode, with a ratio relative to the on-peak cross section of the order of 8% at a center-of-mass energy of 8 TeV. This ratio can be enhanced up to about 20% when a kinematical selection used to extract the signal in the resonant region is taken into account [88]. This arises from the vicinity of the on-shell Z pair production threshold, and is further enhanced at the on-shell top pair production threshold.

In Ref. [89] the authors demonstrated that, with few assumptions and using events with pairs of Z particles, the high invariant mass tail can be used to constrain the Higgs width. For a detailed description, see Ref. [90].

Off-shell measurements are (much) more than consistency checks on Γ_H: observing an excess in the off-shell measurement will be a manifestation of BSM physics, which might or might not need to be in relation with the H width. We need to extend the SM with dynamics, representing an intermediate step toward the next SM, distancing the experimental analysis from repeated refinements due to ever-improving calculations.

How was off-shell production used? First one introduces the notion of ∞-degenerate solutions for the Higgs couplings to SM particles, as done in Ref. [91,89] and uses the fact that the enhanced tail is obviously Γ_H-independent and that this could be exploited to constrain the Higgs width model-independently. Finally, use a matrix element method to construct a kinematic discriminant to sharpen the constraint, see Ref. [92].

More precisely, Refs. [89,93] define the following scenario for on-shell ∞-degeneracy: there is invariance under a scaling of the Higgs couplings and of the total Higgs width defined by

$$\sigma_{i\to H\to f} = (\sigma\cdot BR) = \frac{\sigma_i^{prod}\Gamma_f}{\Gamma_H} \quad \sigma_{i\to H\to f} \propto \frac{g_i^2 g_f^2}{\Gamma_H} \quad g_{i,f} = \xi\, g_{i,f}^{SM},\ \Gamma_H = \xi^4 \Gamma_H^{SM} \tag{23}$$

The gluon fusion production cross section as a function of ZZ invariant mass can be written as:

$$\frac{d\sigma_{gg\to H\to ZZ}}{dm_{ZZ}^2} \sim \frac{g_{ggH}^2 g_{HZZ}^2}{(m_{ZZ}^2 - m_H^2) + m_H^2\Gamma_H^2}. \tag{24}$$

where g_{ggZ} and g_{HZZ} are the couplings of the Higgs boson to gluons and Z bosons, respectively. Integrating either in a small region around m_H, or above the mass threshold $m_{ZZ} > 2m_Z$, where $(m_{ZZ} - m_H) >> \Gamma_H$, the cross sections are, respectively:

$$\sigma_{gg\to H\to ZZ^*}^{on-shell} \sim \frac{g_{ggH}^2 g_{HZZ}^2}{m_H\Gamma_H} \tag{25}$$

$$\sigma_{gg\to H\to ZZ^*}^{on-shell} \sim \frac{g_{ggH}^2 g_{HZZ}^2}{2m_H^2} \tag{26}$$

The cross section for the on-shell production will not change if the squared product of the coupling constants $g_{ggH}^2 g_{HZZ}^2$ and the total width Γ_H are scaled by a common factor r. On the contrary, away from the resonance the cross section is independent of the total width and therefore increases linearly with r. Thus a measurement of the relative off-shell to on-shell production in the $H \to ZZ$ channel provides direct information on Γ_H, as long as the coupling ratios remain unchanged, i.e. the gluon fusion production is dominated by the top-quark loop and there are no new particles contributing.

The final states $H \to ZZ \to 4l$, where one Z boson decays to an e or μ pair and the other to either an e or μ pair, $H \to ZZ \to 2l2\nu$ and and $H \to WW \to 2l2\nu$ have been analysed in ATLAS [94], and CMS [95,96].

The results on the limit on the H width from the analysis of the off-shell H production for the ATLAS and CMS experiments are shown in Fig. 21. The observed 95% CL upper limits on the width are 22.7 and 13 MeV for ATLAS and CMS respectively, while the expected 95% CL upper limits are 33 MeV and 26 MeV. These results have to be compared with the

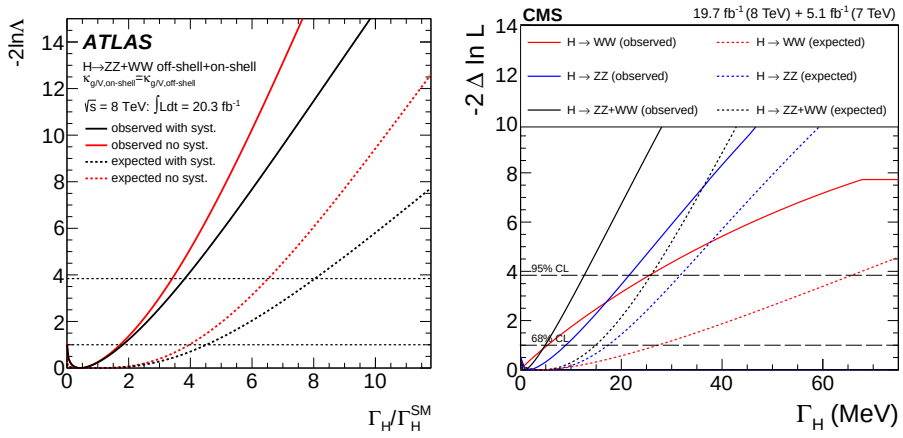

Fig. 21: Scan of the negative log-likelihood as a function of Γ_H/Γ_{SM} (ATLAS) and Γ_H (CMS) for the combined fit of the H → ZZ and H → WW channels at 7 and 8 TeV center of mass energy. The analyses assume the same ggF and VBF ratio of signal strengths.

upper limit on the direct measurement of the width of the H resonance in γγ and 4l final states of about 2 and 3 GeV at 95% CL. The analysis of the off-shell production improves the limits on the Higgs width by a factor of about 100.

After the experiments published their analysis, and with respect to Ref. [90] the following theoretical improvements have been made:

- full next-to-next-to-leading (NNLO) for $\bar{q}q \to VV$, Ref. [97],
- 2-loop amplitudes for massless $gg \to VV$ Refs. [98,99],
- ZZ production in NNLO QCD, Ref. [100].

The 2-loop amplitudes for massive $gg \to VV$ seem out of reach; NLO is known in $1/m_t$-expansion, see Ref. [101]. For off-shell studies in vector boson fusion (VBF) see Ref. [102].

How should off-shell production be used? However, scaling couplings at the H peak is not the same thing as scaling them off-peak; the consequence of this fact is that the kappa framework is not adequate and needs a generalisation, e.g. using SMEFT. Therefore, one should use SMEFT at a given order (possibly NLO) or any other consistent way of describing SM deviations. Using SMEFT as an example, the strategy is:

- write any amplitude as a sum of deformed SM sub-amplitudes and
- add another sum of deformed, non-SM, sub-amplitudes.

The rationale for this course of action (with respect to the original kappa framework) is that physics is symmetry plus dynamics; symmetry is quintessential (gauge invariance, etc.) but symmetry without dynamics does not bring us this far. At LEP the dynamics was SM, the unknowns were $M_{\rm H}\,(\alpha_{\rm s}(M_{\rm Z}),\dots)$, while at LHC (post the Higgs discovery) the unknowns are the SM-deviations but, how to describe dynamics? Selecting a BSM model is a choice but is there something more model independent? The answer is positive: we need a decomposition where dynamics is controlled by amplitudes with known analytical properties and the deviations (with a direct link to UV completions) are ultimately connected to Wilson coefficients.

On-shell studies will tell us a lot, off-shell ones will tell us (hopefully) everything else. We want to study the physics away from the H peak with a SM-deformed theory (up to some reasonable value $E \ll \Lambda$) but we also need to reproduce (deformed) SM low-energy effects, e.g. VV and tt thresholds; BSM loops will remain unresolved, just like SM loops are unresolved in the Fermi theory. That is why one needs to expand SM deformations into a SM basis with the correct (low energy) behaviour: in the neighbourhood of the peak any parameterisation of the deviations will work (certainly at LO), while running off-shell requires a deeper knowledge of the analytical properties of the deformed amplitude.

To summarise, the correct way of describing off-shell SM deviations is

$$\sigma_{\rm EFT}(s) = \mid \kappa_{\rm prod}(s)\,\kappa_{\rm dec}(s) \mid^2 \sigma_{\rm SM}(s)\,, \tag{27}$$

where the "running" kappa parameter (s is the Higgs virtuality) is defined by

$$\kappa_{\rm prod}(s)\,\kappa_{\rm dec}(s) = \mu^{\rm off}_{\rm ZZ}(s)\ . \tag{28}$$

A discussion on $\mu^{\rm off}_{\rm ZZ}(s)$ will be given in Sect. 7.2.2.

Off-shell gauge invariance A final comment on on-shell versus off-shell for LHC physics is needed. There is an important role played by gauge invariance, thus due care is needed in the "signal" definition, i.e, the resonant part. In other words, we meet the usual problems that are present when unstable particles enter the game. Certainly, LHC is not LEP, where only one resonant contribution was present; for a light SM Higgs boson the 4f decays are 40% of the 2f decays, as a consequence we always face the problem of having to deal with many off-shell, unstable, particles, even at the H peak.

The question that we will readdress in Sect. 7 is: how to interpret

$$\Gamma\left(\mathrm{H}\to \mathrm{WW}\to \nu \mathrm{l} \nu' \mathrm{l}'\right) \quad \text{vs.}\ \Gamma\left(\mathrm{H}\to \mathrm{WW}\right), \tag{29}$$

or, stated differently, how to define $\Gamma\left(\mathrm{H}\to \mathrm{WW}\right)$. The short answer is: never introduce quantities that are not well-defined; the Higgs couplings can be extracted from Green's functions in well-defined kinematical limits, e.g. residues of the poles after extracting the

parts which are one-particle irreducible. These are well-defined Quanptum-Field-Theory (QFT) objects, that we can probe both in production and in decays. From this perspective, VH or VBF are on equal footing with ggF and Higgs decays.

7. Theoretical developments

Run 1 at LHC has not shown any direct evidence for new physics and the available studies on the couplings of the 125 GeV resonance show compatibility with the Higgs boson of the SM. What we need, in preparation for the final results of Run 2 and 3, requires a consistent theory of SM deviations and a consistent link between realistic (fiducial) observables and theory parameters, see Refs. [103,104] and Ref. [105].

As discussed in this review, the first attempt to characterise SM deviations is represented by the so-called kappa-framework, introduced in Refs. [26,13].

A very general question that we want to address is: does it make sense to "fit" the EW core? Note that this problem (the LHC problem) is not confined to introducing a specific parametrisation for SM deviations.

At LEP the number of quantities was reduced, implying that some assumption was made on the behaviour of the primordial quantities. The validity of these assumptions was judged on statistical grounds. Within these assumptions, as QED deconvolution and resonance approach (i.e. restricting the process $e^+e^- \to \bar{f}f$ to its Z-resonant component), the secondary quantities, the pseudo-observables (POs), were as "observable" as the first ones.

However, Higgs physics at LHC is radically different from Z physics at LEP, since we have to work with very different scales, e.g. on-shell H decays are very different from, large Q^2, VH production. None of this "complication" existed at LEP. Furthermore, at LHC the EW core (including the Higgs properties) is always embedded into a QCD environment, subject to large perturbative corrections and we certainly expect considerable progress in the "evolution" of these corrections. The same considerations apply to PDFs when studying high-mass (large x) final states. The consequence is that, also for LHC, one has to list the assumptions that are made in studying Higgs couplings and judge them on statistical grounds. To repeat the main argument, the huge QCD background and the associated uncertainty are such that one can fit the data starting from a given parameterisation of the SM deviations but for each new QCD calculation the result will change substantially and not multiplicatively.

The procedure that we are suggesting is: write the answer in terms of SM deviations, after which, certain combinations of the deviation parameters will define the LHC POs and will be fitted. Optimally, part of the factorising QCD corrections could enter the PO definition. As for the framework for deviations, the parametrisation should be as general as possible, with a priori no dropping of terms: this will allow to "reweight" when new (differential) K-factors become available. Parton density functions (PDFs) changing is the most serious

problem. At LEP the e^+e^- structure functions were known to very high accuracy (the effect of using different QED radiators, differing by higher orders treatment, was tested). A change of PDFs at LHC will change the convolution.

Keeping in mind all the caveats in the interpretation of the Higgs couplings, we proceed with a description of POs at LHC since, in our opinion, it will be crucial to follow the path

$$\text{LHC data} \rightarrow \text{POs} \rightarrow \text{SMEFT}.$$

7.1. LHC pseudo-observables

Why going beyond the κ-framework? We can repeat that the κ-parameters are easy to understand in terms of how they change cross sections and partial decay widths (the so-called "peak" observables), but there are theoretical limitations as discussed in Section 5. In this Section we will emphasise that extending the framework is currently seen [28] as expressing the κ-parameters in terms of Wilson coefficients in some Effective Field Theory (i.e. SMEFT). One important point is that electroweak corrections are not defined in the kappa framework if the kappa's are meant as coupling modifiers. In the SMEFT we will have the SM EW corrections plus higher-dimensional operators in EW loops.

The rationale in building a Quantum Field Theory (QFT) of SM-deviations is not so much in the numerical impact of higher orders (however, see Ref. [32] for a nice discussion) but in promoting a phenomenological tool to the full status of QFT. Another reason for having a complete formalism is to avoid a situation where experimenters will have to go back and remove a provisional formalism from the analyses. However, for some of the Wilson coefficients it is hard to understand both qualitatively and quantitatively what some parameter value does to observables; therefore, one question that we would like to answer is the following: could we use and translate part of the LEP language (e.g. the one of POs) to recast parameters into POs?

Any QFT describes dynamics in terms of its Lagrangian parameters. At the LHC (after the discovery) one would like to try a model-independent approach. From LEP to LHC, does history repeat itself? Why should it? The rationale of using POs at LHC is because the POs are a platform between realistic observables and theory parameters [106,107], allowing experimentalists and theorists to meet half way. In principle, ATLAS and CMS should also publish their fiducial and template cross sections since they are alternative and not antithetic to the POs. As already stated, LHC is much more complex than LEP since, as an example, in the study of off-shell Higgs physics, resonant and non-resonant parts are perfectly tied together and there are severe issues of gauge invariance that must be taken into account. Thus, how could we interpret objects like $\Gamma(\mathrm{H} \rightarrow \mathrm{WW}^*)$?

Despite inherent technical difficulties the next physics goal for LHC is high precision study of SM-deviations. Ideally, this would require the following steps:

(1) For each process write down some (QFT-compatible) amplitude allowing for

SM-deviations, both for the resonant part (usually called "signal") and the non-resonant component (usually called "background"); NLO SMEFT is a good example.

(2) Insert the resonant part expressed through POs without neglecting terms and without subtracting the SM background; the background, i.e. the non resonant part, can change as well. The idea is to project some "primordial quantities", say number of observed events in some pre-defined set-up, into some "secondary quantities" closer to the theoretical description of the phenomena. In this step, the number of quantities should not be reduced a priori, unless the validity of the assumptions that have been made on the behavior of the primordial quantities is judged and justified on statistical grounds.

(3) Use fiducial/template observables and fit POs, conventionally defined.

At a later stage, we can derive Wilson coefficients or BSM Lagrangian parameters, publish the full list of fiducial/template (with modern RIVET and HEPDATA technology) and POs *à la* LEP (that will become the LHC legacy).

In the rest of this Section we will summarise the state of art in studying SM deviations.

A list of POs at LHC The complete and most updated reference for POs at LHC can be found in Ref. [108]. A summary table for POs at LHC is the following:

$\mathbf{L_1}$ An external layer of "physical" POs [19] (similar to σ_f^{peak} at LEP):

$$\sum_f \Gamma_{Vff}\,, \quad N_{off}^{41}\,, \quad A_{FB}^{ZZ}\,, \quad \sigma(qq \to ZZjj) \tag{30}$$

etc, where Γ_{Vff} is the partial decay width for $H \to [\text{on-shell}\,V] + \bar{f}f$, N_{off}^{41} is the number of events for $[\text{off-shell}\,H] \to 41$ and A_{FB}^{ZZ} is a forward-backward (FB) asymmetry: for instance, a FB-asymmetry in the angle between the e and the W reconstructed from qq pair in $H \to evqq$ or an F-asymmetry $(\pi/4)$ w.r.t. $|\cos\phi|$, ϕ being the angle between the decay planes of the reconstructed Z bosons, e.g. in the decay $H \to eeqq$. These variables are based on a multi pole expansion (MPE), i.e. these are processes which include a resonance that is fully characterised by the position of the corresponding complex pole, its residue and the regular part in the Laurent expansion around the pole [c]. Furthermore, these "physical" POs are computed without recurring to a zero width approximation or a truncated MPE.

$\mathbf{L_2}$ An intermediate layer of POs (similar to LEP $g_{V\,A}^{e}$), based on quantities that can be extracted from Green's functions in well-defined kinematical limits [109,18,17],

$$\varepsilon_{HVV}^{(1)}\,, \quad \varepsilon_{HVV}^{(2)}\,, \quad \varepsilon_{H\gamma\gamma}, \varepsilon_{H\gamma Z}\,, \quad \varepsilon_{H\bar{f}f}\,, \tag{31}$$

[c] For technical details on MPE, see Ref. [19].

once again based on MPE, analyticity, unitarity, and crossing symmetry. For instance, $\varepsilon^{(1,2)}_{\mathrm{HVV}}$ will be introduced in Eq.(38) and parametrises deviations from the SM in the decay $\mathrm{H} \to \mathrm{VV}$. Once it is "measured" we can compare it with the corresponding SM value or any other specific BSM value. For instance, $\varepsilon_{\mathrm{H}\gamma\gamma}$ refers to the $\mathrm{H} \to \gamma\gamma$ decay, is zero at LO, and is known up to two loops in the SM and up to one loop in many BSM models. Finally, $\varepsilon_{\mathrm{H}\bar{\mathrm{f}}\mathrm{f}}$ refers to the decay $\mathrm{H} \to \bar{\mathrm{f}}\mathrm{f}$, etc. Once the intermediate POs are "measured" their interpretation will be possible. In full generality, a 1PI Green's function with N external (on-shell) lines, carrying Lorentz indices $\mu_i, i = 1, \ldots, \mathrm{N}$ will be decomposed as

$$\mathrm{A}_{\mathrm{proc}} = \sum_{l=1}^{\mathrm{L}} \varepsilon^{l}_{\mathrm{proc}}\, \mathrm{K}^{l}_{\mu_1 \ldots \mu_{\mathrm{N}}}\,, \tag{32}$$

where the set K^l $(l = 1 \ldots \mathrm{L})$ contains independent tensor structures made up of external momenta, metric tensors, elements of the Clifford algebra, and Levi-Civita tensors. Symmetries, including gauge invariance reduce the number of structures, e.g. only one structure in $\mathrm{H} \to \gamma\gamma, \mathrm{Z}\gamma$ (CP-even only) due to Ward identities.

L_3 An internal layer of POs: the generalised kappas. A first example: consider the amplitude for a loop-initiated process, e.g. $\mathrm{H} \to \gamma\gamma$; in the SM it can be decomposed as

$$\mathrm{A}_{\mathrm{H}\to\gamma\gamma} = \mathrm{A}^{\mathrm{f}}_{\mathrm{H}\to\gamma\gamma} + \mathrm{A}^{\mathrm{W}}_{\mathrm{H}\to\gamma\gamma}\,, \tag{33}$$

where the superscript f denotes fermion loops and the superscript W denotes the bosonic part. The kappa-deformed amplitude is characterised by

$$\kappa^{\gamma\gamma}_{\mathrm{f}}\,, \quad \kappa^{\gamma\gamma}_{\mathrm{W}}\,, \quad \kappa^{\gamma\gamma\,\mathrm{nf}}_{i}\,, \quad \text{etc} \tag{34}$$

where the kappa parameters

- with a f subscript multiply the SM fermion sub-amplitude $\mathrm{A}^{\mathrm{f}}_{\mathrm{H}\to\gamma\gamma}$,
- those with a W subscript multiply the SM bosonic sub-amplitude $\mathrm{A}^{\mathrm{W}}_{\mathrm{H}\to\gamma\gamma}$,
- those with a nf superscript refer to a set of non-factorisable sub-amplitudes that are computable in SMEFT and are not present in the original kappa framework. These amplitudes are better defined in the context of the SMEFT, e.g. see Eq.(49).

Note that these kappa parameters have an additional label specifying the process, therefore $\kappa^{\gamma\gamma}_{\mathrm{f}} \neq \kappa^{\mathrm{Z}\gamma}_{\mathrm{f}}$ etc. For tree initiated processes the generalised kappa parameters have another label, distinguishing LO from NLO, see Eq. (141) and Eqs. (173-175) of Ref. [31] for details. The introduction of generalised kappas is not limited to decay processes; for instance, consider $\bar{\mathrm{q}}\mathrm{q} \to \mathrm{ZH}$, where we can write

$$\mathrm{A}_{\bar{\mathrm{q}}\mathrm{q}\to\mathrm{HZ}} = g^2 \left(1 + \Delta\kappa^{\bar{\mathrm{q}}\mathrm{q}\to\mathrm{HZ}}\right) \mathrm{A}^{\mathrm{LO}}_{\bar{\mathrm{q}}\mathrm{q}\to\mathrm{HZ}} + g^2 \sum_{\substack{\lambda=\pm \\ i=1,2}} \bar{\mathrm{v}}\, \gamma^{\mu}\, \gamma_{\lambda}\, \mathrm{u}\, e^{\nu}\, \Delta\kappa^{\bar{\mathrm{q}}\mathrm{q}\to\mathrm{HZ};\mathrm{nf}}_{\lambda\, i}\, \mathrm{A}^{i}_{\mu\nu}\,,$$

$$\gamma_\pm = \frac{1}{2}(1 \pm \gamma^5), \qquad \mathrm{A}^1_{\mu\nu} = \delta_{\mu\nu}, \quad \mathrm{A}^2_{\mu\nu} = p_{\mathrm{Z}\mu}\, p_{\mathrm{H}\nu}, \tag{35}$$

and e^μ is the Z polarisation vector and

$$\mathrm{A}^{\mathrm{LO}}_{\bar{\mathrm{u}}\mathrm{u}\to\mathrm{HZ}} = \frac{1}{8}\frac{M_\mathrm{W}}{\mathrm{c}^3_\theta}\sum_{\lambda=\pm}(1+\lambda-\frac{8}{3}\mathrm{s}^2_\theta)\,\bar{\mathrm{v}}\not{e}\gamma_\lambda\,\mathrm{u}\,,\ \text{etc}\,. \tag{36}$$

Similar decompositions can be provided for $\mathrm{qq}\to\mathrm{qqH}$, $\mathrm{gg}\to\bar{\mathrm{t}}\mathrm{tH}$, etc.

To summarise, the generalised kappa parameters are a convenient way to combine Wilson coefficients, i.e. for a given group of observables the set of Wilson coefficients collapses into a set of generalised kappas. Of course, the exact relation between generalised kappas and Wilson coefficients depends on the order of the SMEFT calculation, LO or NLO.

$\mathrm{L_4}$ Finally, the innermost layer: the Wilson coefficients in SMEFT (LO or NLO) or non-SM parameters in BSM (e.g. mixing angles α,β, soft-breaking scale, M_{sb}, etc., in THDMs).

As we will explain in more detail below, introducing the innermost layer is an operation that can be eventually postponed. The original work on intermediate POs at LHC can be found in Refs. [109,18,17] and in Ref. [19] for external POs.

Intermediate layer ($\mathrm{L_2}$) In the following we give few examples, starting with the intermediate layer, Eq.(31). The amplitude for the Higgs decay $\mathrm{H}\to\gamma(p_1)\gamma(p_2)$ can be parametrised as

$$\mathrm{A}_{\mathrm{H}\to\gamma\gamma} = \varepsilon_{\mathrm{H}\gamma\gamma}\,\frac{p_1\cdot p_2\, g^{\mu\nu} - p_2^\mu p_1^\nu}{M_\mathrm{H}}\,, \tag{37}$$

Another example where we use MPE is the following:

$$\mathrm{A}_{\mathrm{H}\to\mathrm{VV}} = \varepsilon^{(1)}_{\mathrm{HVV}}\, M^2_\mathrm{H}\, g^{\mu\nu} + \varepsilon^{(2)}_{\mathrm{HVV}}\, p_2^\mu\, p_1^\nu\,. \tag{38}$$

In all cases the Higgs production parametrization follows by using analyticity and crossing symmetry. In any process, the residues of the poles corresponding to internal, unstable particles are numbers, while the non-resonant part is a multivariate function that requires some basis, i.e. a less model independent theory of SM deviations. That is to say, residues of the poles (MPE) can be intermediate POs by themselves. Numerically speaking, the residue of the pole depends on the impact of the non-resonant part which is small in gluon-fusion but not in Vector Boson Scattering. Therefore, the focus for reporting data should always be on real observables, fiducial/template cross sections, and pseudo-observables. To give an idea of the general structure we consider the $\mathrm{H}\to 4\,\mathrm{f}$ channels: including CP-odd couplings, there are 3 flavor-universal charged-current POs, 7 flavor-universal neutral-current POs, and a set of flavor non-universal charged-current POs; the number of non-universal POs depends on the fermion species we are interested in [108].

Few additional definitions are needed to appreciate the consistency of the whole theoretical construction. Here, we only provide a brief summary, with the corresponding references.

- By on-shell S-matrix for an arbitrary process (involving external unstable particles) we mean the corresponding (amputated) Green's function supplied with LSZ factors and sources, computed at the (complex) poles of the external lines [110,12]. Processes that involve stable particles can be straightforwardly transformed into a physical PO.

- The connection of the HVV, $V = Z, W$ (on-shell) S-matrix with the off-shell vertex $H \to VV$ and the full process $pp \to 4f$ is more complicated and is discussed in some detail in Sect. 3 of Ref. [19]. The "on-shell" S-matrix for HVV, being built with the the residue of the $H-V-V$ poles in $pp \to 4f$ is gauge invariant by construction (it can be proved by using Nielsen identities) and represents one of the building blocks for the full process: in other words, HVV is a PO.

- Technically speaking the "on-shell" limit for external legs should be understood "to the complex poles" (for a modification of the LSZ reduction formulas for unstable particles see Ref. [111]) but, as well known, at one loop we can use on-shell masses (for unstable particles) without breaking the gauge parameter independence of the result.

- It is worth noting that there are subtleties when the H is off-shell. They are described in Appendix C.1 of Ref. [12]. Briefly, there is a difference between performing an analytical continuation (H virtuality $\to$ H on-shell mass) in the off-shell decay width and using leading-pole approximation (LPA) of Ref. [112], i.e. the doubly-resonant part, where the matrix element (squared) is projected but not the phase-space. Analytical continuation is a unique, gauge invariant procedure, the advantage of leading-pole approximation is that it allows for a straightforward implementation of experimental cuts.

External layer (L_1) The external layer, Eq.(30), requires additional work. It would be ideal to stop reporting non existing objects, e.g. $H \to ZZ$ or non-gauge-invariant objects, e.g. $H \to Z^*Z$. The external layer, i.e. the "physical" POs, allows for experimental cuts and thus bypasses ad hoc constructions like "diagram removal" (not gauge invariant) or "diagram subtraction" (with ad hoc prefactors and Breit-Wigner profiles).

MPE is the tool for isolating gauge invariant parts of any amplitude, therefore it is enough to construct quantities in the intermediate layer. Quantities in the external layer aim to identify "elementary" subprocesses inside a "realistic" processes, e.g. simple production/decay processes inside realistic processes, e.g. $\bar{t}tH$ production inside WbWb production. MPE, i.e. gauge-invariant splitting of the amplitude, is not the same as "factorisation" of the process into sub-processes; let us explain what it is meant by requiring the pole to be inside

the physical region. The propagator and phase-space are

$$|\Delta|^2 = \frac{1}{\left(s-M^2\right)^2+\Gamma^2 M^2} = \frac{\pi}{M\Gamma}\,\delta\left(s-M^2\right) + \mathrm{PV}\left[\frac{1}{\left(s-M^2\right)^2}\right],$$
$$d\Phi_n\left(P,p_1\ldots p_n\right) = \frac{1}{2\,\pi}\,dQ^2\,d\Phi_{n-(j+1)}\left(P,Q,p_{j+1}\ldots p_n\right)\,d\Phi_j\left(Q,p_1\ldots p_j\right), \quad (39)$$

where PV denotes the principal value (understood as a distribution, see Ref. [113]). It would be convenient to define POs through a factorisation of the process into sub-processes, e.g. by "isolating" the production and decay of a particle of momentum Q. A typical example is the "isolation" of $\mathrm{H}\to\mathrm{Z}\gamma$ in $\mathrm{H}\to\bar{\mathrm{f}}\mathrm{f}\gamma$, where $\mathrm{H}\to\mathrm{Z}\gamma$ will be the relevant PO [114]. However, to "complete" the Q-decay (requiring $d\Phi_j$), we need the δ-function in Eq.(39). We can say that the δ-part of the resonant (squared) propagator "opens" the corresponding line and allows us to define POs; however, this is not the case for t-channel propagators, which cannot be cut. Note that the pole must be inside the allowed portion of phase space which is not always the case when experimental cuts are introduced or the kinematics of the process does not allow it. For instance, $\Gamma(\mathrm{H}\to\mathrm{Z}\gamma)$ can be promoted to be a "physical" PO whereas $\Gamma(\mathrm{H}\to\mathrm{ZZ})$ cannot and we should introduce $\sum_{\mathrm{f}}\Gamma(\mathrm{H}\to\mathrm{Z}\bar{\mathrm{f}}\mathrm{f})$. As an additional example, consider the process $\mathrm{qq}\to\bar{\mathrm{f}}_1\mathrm{f}_1\bar{\mathrm{f}}_2\mathrm{f}_2 jj$: given the structure of the resonant poles we can define different POs, e.g.

$$\sigma(\mathrm{qq}\to\bar{\mathrm{f}}_1\mathrm{f}_1\bar{\mathrm{f}}_2\mathrm{f}_2 jj) \overset{PO}{\longmapsto} \sigma(\mathrm{qq}\to\mathrm{H}jj)\,\mathrm{Br}(\mathrm{H}\to\mathrm{Z}\bar{\mathrm{f}}_1\mathrm{f}_1)\,\mathrm{Br}(\mathrm{Z}\to\bar{\mathrm{f}}_2\mathrm{f}_2),$$
$$\sigma(\mathrm{qq}\to\bar{\mathrm{f}}_1\mathrm{f}_1\bar{\mathrm{f}}_2\mathrm{f}_2 jj) \overset{PO}{\longmapsto} \sigma(\mathrm{qq}\to\mathrm{ZZ}jj)\,\mathrm{Br}(\mathrm{Z}\to\bar{\mathrm{f}}_1\mathrm{f}_1)\,\mathrm{Br}(\mathrm{Z}\to\bar{\mathrm{f}}_2\mathrm{f}_2). \quad (40)$$

There are additional fine points to be considered when factorising a process into "physical" sub-processes, and details have been discussed in Ref. [19].

The internal and innermost layers require the introduction of SMEFT.

7.2. Standard Model Effective Field Theory

The basis for NLO calculus of the Standard Model effective field theory (SMEFT) has been developed in Ref. [31] and in Refs. [32,33]. The issue of theoretical uncertainty associated with missing higher orders has been raised and discussed in Ref. [70]. The interplay between SMEFT and pseudo-observables has been introduced in Ref. [19].

In Ref. [31] one can find all technical details as well as the full list of counterterms and mixings that are relevant for Higgs physics. The SMEFT used is based on the assumption of one Higgs doublet with a linear representation; for non-linear representations see Refs. [115,83]. There are two different research approaches in any EFT, the top-down and bottom-up approach.

7.2.1. *The top-down approach*

The top-down approach starts with a known theory and systematically eliminates degrees of freedom associated with energies above some energy scale Λ. The construction of a low-energy effective theory is, in general, not simple for the high-energy degrees of freedom may be tangled up with the low-energy ones. For a distinction between Wilsonian and "continuum" EFT see Ref. [116].

The integration of heavy fields in a wide class of BSM models, containing more that one representation for scalars has been discussed in Refs. [117,118,60,119,120].

The authors of Ref. [121] have discussed the conditions for an effective field theory to give an adequate low-energy description of the underlying physics beyond the SM. Starting from the EFT where the SM is extended by dim = 6 operators, experimental data can be used without further assumptions to measure (or set limits on) the EFT parameters. Their conclusion is that interpretation of these results requires instead a set of broad assumptions on the UV dynamics.

The work of Refs. [83,84] shows how the Higgs couplings analysis of Run 1 can be expanded into a Higgs operator analysis, based on a linearly-realised dim = 6 Lagrangian. The extraction of the corresponding Wilson coefficients from Run 1 data is discussed emphasising how kinematic distributions can be included and how they affect the extraction of the Wilson coefficients. Even more important, they study how well weakly interacting extensions of the Higgs and gauge sector are described by such a dim = 6 Lagrangian. It turns out that in spite of the lacking scale hierarchy the dim = 6 approximation quantitatively captures the relevant features of the full models, except for the appearance of new resonances.

SMEFT is a double expansion in $g^2\,\mathrm{v}^2/\Lambda^2$ and $g^2 E^2/\Lambda^2$, where v is the Higgs VEV and E is the typical energy scale at which the measurement is performed. Operators controlled by the VEV do not change kinematic distributions. The general argument, discussed in Refs. [83], is the following: for a "reasonable" weakly interacting theory, when only studying total rates with an LHC accuracy of 10%, the LO impact can be estimated according to:

$$\left| \frac{\sigma \times \mathrm{BR}}{(\sigma \times \mathrm{BR})_{\mathrm{SM}}} - 1 \right| = \frac{g^2 M_{\mathrm{H}}^2}{\Lambda^2} > 10\% \tag{41}$$

that implies

$$\Lambda < \frac{g M_{\mathrm{H}}}{\sqrt{10\%}} \approx 400\ GeV\ . \tag{42}$$

This explains why differential distributions are essential, involving a new scale $g\,p_{\mathrm{T}}/\Lambda$. There is always a huge improvement on the sensitivity when using differential distributions as can be seen by comparing the constraints obtained in the measurement of the signal strength with the ones including distributions.

Ref. [61] makes the point that, for the new physics scales accessible at the LHC, the effective operator expansion is only relatively slowly converging. For tree-level processes, the

agreement between SMEFT and a range of UV-complete models depends sensitively on the appropriate definition of their matching. To be more precise consider a theory with both light and heavy particles; the Lagrangian depends on M, the mass of the heavy degree of freedom. Next, introduce the corresponding effective theory, valid up to a scale $\Lambda = M$. Afterwards we renormalise the two theories, say in the $\overline{\rm MS}$-scheme (taking care that loop-integration and heavy limit are operations that do not commute), and impose "matching" conditions among renormalised "light" 1 particle irreducible (1PI) Green's functions [d], i.e.

$$\Gamma^{\rm R}(\mu)\,|_{\rm full}\,(\mu) = \Gamma^{\rm R}(\mu)\,|_{\rm eff}\,, \qquad \mu \leq M\,, \tag{43}$$

where μ is the renormalisation scale and $\Gamma_{\rm R}$ is any renormalised Green's function. At the one-loop level, near the scale of EWSB the validity of SMEFT description can be systematically improved through an appropriate matching procedure.

7.2.2. *The bottom-up approach*

Finding deviations is what we expect, at least experimentally; in that sense we should place more focus on measuring them than in just setting limits. In any (strictly) renormalisable theory with n parameters one needs to match n data points and the $(n+1)$th calculation becomes a prediction. In the SMEFT there are $({\rm N}_6{+}{\rm N}_8{+}\cdots = \infty)$ renormalised Wilson coefficients (where ${\rm N}_n$ is the number of Wilson coefficients of dim $= n$) that have to be fitted, measuring SM deformations due to a single $\mathscr{O}^{(6)}$ insertion. A basis for dim $= 6$, the so-called Warsaw basis, has been provided in Ref. [123]. Recent progress for dim $= 8$ operators can be found in Refs. [124,125,126]. By dim $= 6$ SMEFT basis we mean any set of gauge invariant, dimension 6 operators, none of which is redundant. For a formal definition of redundancy see Sect. 3 of Ref. [27].

SMEFT Lagrangian The treatment of EFT was pioneered in [127,128,129]; the SMEFT approach is based on the following Lagrangian:

$$\mathrm{A} = \sum_{n=\mathrm{N}}^{\infty} g^n\,\mathrm{A}_n^{(4)} + \sum_{n=\mathrm{N}_6}^{\infty}\sum_{l=1}^{n}\sum_{k=1}^{\infty} g^n\,g_{4+2k}^{l}\,\mathrm{A}_{n,l,k}^{(4+2k)}\,, \tag{44}$$

where g is the $SU(2)$ coupling constant and $g_{4+2k} = 1/(\sqrt{2}G_{\rm F}\Lambda^2)^k = g_6^k$; $G_{\rm F}$ is the Fermi coupling constant and Λ is the scale around which new physics (NP) must be resolved. For each process, N defines the dim $= 4$ Lagrangian at LO (e.g. $N = 1$ for $\mathrm{H} \to \mathrm{VV}$, etc., but $N = 3$ for $\mathrm{H} \to \gamma\gamma$). $N_6 = N$ for tree initiated processes and $N - 2$ for loop initiated ones.

A simple SMEFT ordertable for tree-initiated $1 \to 2$ processes is available in Ref. [28], where the complete definition of LO SMEFT, NLO SMEFT, and MHOU (missing higher order uncertainties) for SMEFT is presented. Here it will suffice to say that for a decay $1 \to 2$,

[d] For a complete definition of the matching procedure see Sect. 3.1 of Ref. [122].

$g\,g_6\,\mathrm{A}^{(6)}_{1,1,1}$ defines the LO SMEFT expression while $g^3\,g_6\,\mathrm{A}^{(6)}_{3,1,1}$ defines the NLO SMEFT amplitude in the perturbative expansion.

NLO corrections are a necessary consequence of the SMEFT being a well-defined field theory. The *numerical size of the higher order terms* depends upon the high energy (UV) scenario dictating the coefficients and Λ, which is unknown. Restricting to a particular UV case is not an integral part of a general SMEFT treatment and various cases can be chosen once the general calculation is performed. All explicit references to the underlying theory are introduced via the matching procedure in the standard approach to EFTs and power counting, see Refs. [127,128,129,130,122,131,132,133,134,135,136,137,138,139,140,141,142,143] for reviews.

SMEFT is a double expansion: in g and $g_6 = \mathrm{v}_\mathrm{F}^2/\Lambda^2$ for pole observables and in $g, g_6\,E^2/\mathrm{v}_\mathrm{F}^2$ for off-shell ones.

To summarize, LO SMEFT refers to dim $= 6$ operators in tree diagrams, sometimes called "contact terms", while NLO SMEFT refers to one loop diagrams with a single insertion of dim $= 6$ operators. One can make additional assumptions by introducing classification schemes in SMEFT. One example of a classification scheme is the Artz-Einhorn-Wudka "potentially-tree-generated" (PTG) scenario [144,27]. In this scheme, it is argued that classes of Wilson coefficients for operators of dim $= 6$ can be tree level, or loop level (suppressed by $g^2/16\pi^2$)[e]. In these cases, the expansion is reorganised in terms of "tree-generated" (TG) (we assume a BSM model where PTG is actually TG) and LG insertions (i.e. "loop-generated"), i.e. LG contact terms and one loop TG insertions, one loop LG insertions and two loop SM etc. It is clear that LG contact terms alone do not suffice.

Strictly speaking we are considering here the virtual part of SMEFT, under the assumptions that LHC POs are defined *à la* LEP, i.e. when QED and QCD corrections are deconvoluted. Otherwise, the real (emission) part of SMEFT should be included and it can be shown that the infrared/collinear part of the one-loop virtual corrections and of the real ones respect factorisation: the total = virtual + real is IR/collinear finite at $\mathcal{O}(g^4\,g_6)$, see Ref. [28].

It is worth noting that SMEFT has limitations, obviously the scale should be such that $E \ll \Lambda$. Understanding SM deviations in tails of distributions requires using SMEFT only up to the point where it stops to be valid, or using the kappa–BSM-parameters connection, i.e. replace SMEFT with BSM models, optimally matched to SMEFT at lower scales. It is worth noting the complementarity between "pole" vs. "tail" measurements: operators that influence tail observables are not the same affecting pole observables, i.e. derivative vs. non-derivative operators. Furthermore, the SMEFT does break down in the tails if you have a cutoff scale that is not outside the larger probe scale. We can say that, eventually, the SM will break in "tails"; projecting into the SMEFT will have a large intrinsic uncertainty, i.e. we do not know what exactly is going on because the SMEFT interpretation becomes a series expanded in a parameter larger than 1.

[e]This classification scheme corresponds only to a subset of weakly-coupled and renormalisable UV physics cases.

To explain SMEFT in a nutshell (for a complete description see Ref. [34]) consider a process described by some SM amplitude

$$\mathrm{A_{SM}} = \sum_{i=1,n} \mathrm{A_{SM}^{(i)}}\,, \tag{45}$$

where i labels gauge-invariant sub-amplitudes. In order to construct the SMEFT one has to select a set of higher-dimensional operators and to start the complete procedure of renormalization. Of course, different sets of operators can be interchangeable as long as they are closed under renormalization. It is a matter of fact that renormalization is best performed when using the so-called Warsaw basis, see Ref. [123]. Moving from SM to SMEFT we obtain

$$\mathrm{A_{SMEFT}^{LO}} = \sum_{i=1,n} \mathrm{A_{SM}^{(i)}} + i\,g_6\,\kappa_\mathrm{c}\,, \qquad \mathrm{A_{SMEFT}^{NLO}} = \sum_{i=1,n} \kappa_i\,\mathrm{A_{SM}^{(i)}} + i\,g_6\,\kappa_\mathrm{c} + g_6 \sum_{i=1,\mathrm{N}} a_i\,\mathrm{A_{nfc}^{(i)}}\,, \tag{46}$$

where $g_6^{-1} = \sqrt{2}\,G_\mathrm{F}\,\Lambda^2$. The last term in Eq.(46) collects all loop contributions that do not factorize and the coefficients a_i are Wilson coefficients. The κ_i start from one, i.e. $\kappa_i = 1 + \Delta\kappa_i$, and the $\Delta\kappa_i$ are linear combinations of the a_i. We conclude that Eq.(46) gives the correct generalization of the original κ-framework at the price of introducing additional, non-factorizable, terms in the amplitude.

Finally, we would like to clarify certain points regarding the following question: do we necessarily have to make UV assumptions? The work in Ref. [121] discusses the conditions for an EFT to give an adequate low-energy description of an underlying physics beyond the SM. The claim is that one has to make a set of broad assumptions on the UV dynamics as one cannot just use SMEFT without UV assumptions (if not for setting limits on the Wilson coefficients). We agree with the view presented in Ref. [143]: the pattern of suppressions for Wilson coefficients is not a SMEFT prediction but must be determined experimentally. Of course, it depends on the underlying UV completion but can be determined experimentally solely by using "low-energy" measurements that can be computed by using SMEFT, as was always done in the past.

SMEFT vs. original kappa framework, the internal layer ($\mathrm{L_3}$) For a discussion of the internal layer, Eq.(34), we consider the present implementation of coupling modifiers, as illustrated in Eq.(9). In general, for $\mathrm{gg} \to \mathrm{H}$ we can use the following decomposition,

$$\mathrm{A^{gg}} = \sum_{\mathrm{q=t,b}} \kappa_\mathrm{q}^\mathrm{gg}\,\mathrm{A_q^{gg}} + \kappa_c^\mathrm{gg}\,, \tag{47}$$

$\mathrm{A_t^{gg}}$ being the SM t-loop etc. The contact term (which is the LO SMEFT) is given by κ_c^gg. Furthermore

$$\kappa_\mathrm{q} = 1 + \Delta\kappa_\mathrm{q} = 1 + g_6\,\delta_\mathrm{q}\,. \tag{48}$$

The innermost layer: Wilson coefficients (L_4) In the context of NLO SMEFT Eq.(47) is rewritten as

$$\begin{aligned} A_{EFT}^{gg} &= \sum_{q=t,b} \kappa_q^{gg} A_q^{gg} + K a_{\phi G} + \sum_{q=t,b} A_q^{nf;gg} a_{qG} \\ &= \frac{g\, g_S}{\pi^2} \sum_{q=t,b} \kappa_q^{gg} A_q^{gg} + 2 g_S\, g_6\, \frac{s}{M_W^2}\, a_{\phi G} + \frac{g\, g_S^2\, g_6}{\pi^2} \sum_{q=t,b} A_q^{nf;gg} a_{qG}\,, \end{aligned} \tag{49}$$

where the κ are linear combination of Wilson coefficients, denoted by a following the Warsaw basis convention. At NLO, $\Delta\kappa = g_6\, \delta$ and

$$\begin{aligned} & g_6^{-1} = \sqrt{2}\, G_F \Lambda^2\,, \quad 4\pi\, \alpha_s = g_S^2 \\ & \delta_t^{gg} = a_{\phi W} + a_{t\phi} + 2 a_{\phi\Box} - \frac{1}{2} a_{\phi D}\,, \qquad \delta_b^{gg} = a_{\phi W} - a_{b\phi} + 2 a_{\phi\Box} - \frac{1}{2} a_{\phi D}\,. \end{aligned} \tag{50}$$

In Eq.(50) $a_{\phi W}$ is LG, as well as $a_{\phi G}$ and a_{qG}. Therefore,

$$\delta_t^{gg}\,|_{PTG} = a_{t\phi} + 2 a_{\phi\Box} - \frac{1}{2} a_{\phi D} \quad \text{,etc.} \tag{51}$$

Remark Instead of the two parameters appearing in Eq.(9) we now have t, b modifiers (containing both PTG and LG), a (LG) contact term and (LG) non factorisable contributions. In order to compare with Eq.(9) we introduce

$$\begin{aligned} & X_{t,b} = |\, A_{t,b}\,|^2\,, \quad X_{tb} = 2\,\mathrm{Re}\left[A_t^\dagger A_b\right], \quad X_q = |\sum_{q=t,b} A_q\,|^2 \\ & Y_t = 2\,\mathrm{Re}\, A_t\,, \quad Y_b = 2\,\mathrm{Re}\, A_b\,, \quad Y_q = 2 \sum_{q=t,b} \mathrm{Re}\, A_q\,, \end{aligned} \tag{52}$$

and derive the results of Tab. 5.

Table 5: Resolved scaling factor in $gg \to H$. K is the coefficient of the contact term as introduced in Eq.(49).

Framework	Scaling factor
κ	$\kappa_t^2 X_t + \kappa_b^2 X_b + \kappa_t \kappa_b X_{t,b}$
LO SMEFT	$X_q + K^2 a_{\phi G}^2 + K a_{\phi G} Y_q$
NLO SMEFT PTG	$\kappa_t^2 X_t + \kappa_b^2 X_b + \kappa_t \kappa_b X_{t,b} + K^2 a_{\phi G}^2 + K a_{\phi G} \kappa_t Y_t + K a_{\phi G} \kappa_b Y_b$

When going interpretational we make additional assumptions: for instance, use NLO SMEFT, adopt the Warsaw basis and eventually work in the Einhorn-Wudka PTG scenario. Options are:

- LO SMEFT: $\kappa_q = 1$ and $a_{\phi G}$ being LG is scaled by $1/16\pi^2$;
- NLO PTG-SMEFT: $\kappa_q \neq 1$ but only PTG operators inserted in loops (non-factorisable terms absent), $a_{\phi G}$ scaled as above;

- NLO full-SMEFT: $\kappa_q \neq 1$, LG/PTG operators inserted in loops (non-factorisable terms present), LG coefficients scaled as above.

Summarising: relaxing the PTG assumption introduces non-factorisable sub-amplitudes proportional to a_{tg}, a_{bg} with a mixing among $\{a_{\phi G}, a_{tg}, a_{bg}\}$. Meanwhile, renormalisation has made one-loop SMEFT finite, e.g. in the G_F-scheme, with a residual μ_R-dependence.

A connection between intermediate POs, generalised kappas, and Wilson coefficients has been derived in Sect. 8 of Ref. [108].

Off-shell SMEFT Consider $H \to ZZ$ for a Higgs of virtuality s. The amplitude is decomposed into Lorentz structures,

$$A^{\mu\nu}_{ZZ} = \mathscr{D}_{ZZ}\, \delta^{\mu\nu} + \mathscr{P}_{ZZ}\, p_2^\mu\, p_1^\nu\,, \tag{53}$$

with the following result:

$$\mathscr{D}_{ZZ} = g\, \kappa^{ZZ}_{LO}\, \mathscr{D}^{LO}_{ZZ} + \frac{g^3}{16\pi^2} \sum_{i=t,b,W} \kappa^{ZZ;D}_{NLO;i}\, \mathscr{D}^{LO;i}_{ZZ} + \frac{g^3 g_6}{16\pi^2} \sum_{a\in A_{ZZ}} \mathscr{D}^{LO;nfc;a}_{ZZ}\, a\,, \tag{54}$$

$$\mathscr{P}_{ZZ} = 2\,\frac{g g_6}{M_W}\, a_{ZZ} + \frac{g^3}{16\pi^2} \sum_{i=t,b,W} \kappa^{ZZ;P}_{NLO;i}\, \mathscr{P}^{LO;i}_{ZZ} + \frac{g^3 g_6}{16\pi^2} \sum_{a\in A_{ZZ}} \mathscr{P}^{LO;nfc;a}_{ZZ}\, a\,. \tag{55}$$

Once again, κ^{ZZ}_{LO} etc. start from one, $\Delta\kappa^{ZZ}_{LO}$ etc. parametrise SM deviations and $\mathscr{D}^{LO}_{ZZ}$ etc. are computed within the SM. Following Eq.(48) the kappas are determined by

$$\begin{aligned}
\delta^{ZZ}_{LO} &= 2\,a_{\phi\Box} + s^2_\theta\, a_{AA} + s_\theta\, c_\theta\, a_{AZ} + \Big[4 + c^2_\theta\,(1 - \frac{s}{M^2_W})\Big]\, a_{ZZ}\,,\\
\delta^{ZZ;D}_{NLO;W} &= 2\,a_{\phi\Box} + \frac{1}{12}\,\frac{1+4\,c^2_\theta}{c^2_\theta}\, a_{\phi D} + s^2_\theta\, a_{AA} + \frac{1}{3}\, s_\theta\,(\frac{5}{c_\theta} + 9\,c_\theta)\, a_{AZ} + (4 + c^2_\theta)\, a_{ZZ}\,,\\
\delta^{ZZ;D}_{NLO;t} &= a_{t\phi} + 2\,a_{\phi\Box} - \frac{1}{2}\, a_{\phi D} + 2\,a_{ZZ} + s^2_\theta\, a_{AA}\,,\\
\delta^{ZZ;D}_{NLO;b} &= -a_{b\phi} + 2\,a_{\phi\Box} - \frac{1}{2}\, a_{\phi D} + 2\,a_{ZZ} + s^2_\theta\, a_{AA}\,,
\end{aligned} \tag{56}$$

$$\begin{aligned}
\delta^{ZZ;P}_{NLO;t} &= \delta^{ZZ;D}_{NLO;t}\,,\\
\delta^{ZZ;P}_{NLO;b} &= \delta^{ZZ;D}_{NLO;b}\,,\\
\delta^{ZZ;P}_{NLO;W} &= 4\,a_{\phi\Box} + \frac{5}{2}\, a_{\phi D} + 3\, s^2_\theta\, a_{AA} + 12\, a_{ZZ}\,.
\end{aligned} \tag{57}$$

Results for the probability distribution of SM deviations are shown in Fig. 22. Here the Wilson coefficients are distributed according to unif$(-1, 1)$ for a scale $\Lambda = 3\ TeV$. Consider a measure of deviation from the SM prediction written as $R = \Gamma_{NLOSMEFT}/\Gamma_{SM} - 1$, where $\Gamma = \Gamma(H \to \gamma\gamma)$. Allowing each Wilson coefficient to have a uniform probability distribution in a interval $I_n = [-n, +n]$, the result from sampling random values for the Wilson

coefficients and calculating R at LO and NLO produces results that are substantially different. This demonstrates how the LO and NLO procedures inherently allow for and lead to different inferences on the Wilson coefficients.

Moving from kappa fits to PO, SMEFT fits .

In LEP times, the experimental collaborations followed a complete path, i.e. primordial quantities (PQs) $\rightarrow$ pseudo-observables (POs) $\rightarrow$ couplings. Primordial quantities are obtained through many assumptions, event classification, detector response, etc. On the observability of POs we can say that all quantities are equally "observable" provided one endorses the conceptual description of the phenomena that they are supposed to quantify.

It is foreseeable that ATLAS and CMS, given the more complex environment at LHC, will only do PQs $\rightarrow$ "something" and the big decision will be about "something" and "how". Let's assume that the analysis will concentrate on extracting Wilson coefficients (W), as

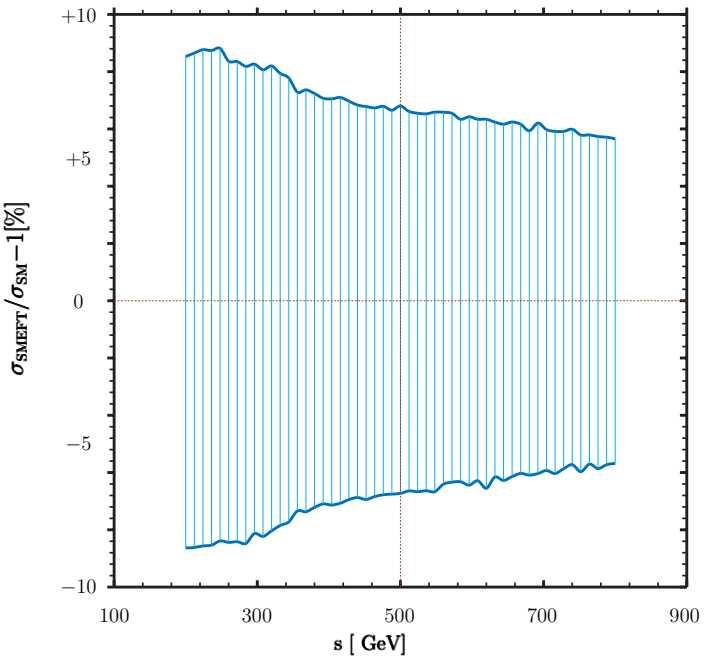

Fig. 22: Off-shell gg $\rightarrow$ H. The Higgs virtuality is s and Wilson coefficient are generated with support $|\, a_i \,| \in [-1\,,+1]$ (unif$(-1\,,1)$). $\Lambda = 3\ TeV$.

done in Run 1 for PQs $\to$ kappa ratios. Let's examine some of the consequences: assuming a (possible) experimental choice given by PQs $\to$ $\mathrm{W_{LO}}$, we will miss the intermediate step PQs $\to$ POs $\to$ W; therefore we will not be able to undo the analysis, e.g. to derive NLO Wilson coefficients from LHC data. Furthermore, the extraction at LO will be based on some "LO" procedure and little additional knowledge will be available because everything will be hard-coded somewhere inside some code. Once again, for this reason, nobody will be able to unfold the $\mathrm{W_{LO}}$, i.e. $\mathrm{W_{LO}}$ $\to$ POs $\to$ something else. For this reason we want to emphasize that

a) PQs $\to$ POs is crucial while PQs $\to$ W should be viewed as subsidiary,

b) PQs $\to$ $\mathrm{W_{LO}}$, if done directly, should be done with a general/consistent procedure, i.e. any LO procedure used should be extendible to NLO. Therefore the use of "LO" should be restricted to the lowest-order prediction of a, fully consistent, theory and not used as a synonym, essentially meaning "phenomenological approach".

The advantages in upgrading the (original) kappa fits are obvious: on the theory side the extension allows us to systematically include loop corrections, not only in QCD; on the experimental side it becomes possible to describe modified kinematic distributions, like for example the transverse momentum of the Higgs. Finally, on the theory and experimental sides, it allows us to combine measurements in the Higgs sector with any search for physics beyond the SM.

7.3. Motivations for an EFT approach

The lesson of the experiments from 1973 to today is that it is extremely difficult to find a flaw in the SM, thus maybe the SM includes elements of a truly fundamental theory. But then how can one hope to make theoretical progress without experimental guidance? One should pay close attention to what we do not understand precisely about the SM even if the standard prejudice is that it is a hard technical problem, and solving it won't change anything. The conventional vision is that some very different physics occurs at the Planck scale and the SM is just an effective field theory. It is possible that at some very large energy scale, all non-renormalisable interactions disappear. This seems unlikely, given the difficulty with gravity. It is possible that the rules change drastically. It may even be possible that there is no end, simply more and more scales. This prompts the important question whether there is a last fundamental theory in this tower of EFTs which supersede each other as energy rises. Some people conjecture that this deeper theory could be a string theory, i.e. a theory which is not a field theory any more. Or should one ultimately expect from physics theories that they are only valid as approximations and in a limited domain (see Ref. [145])? Alternatively, the approach could be that one should not resort to arguments involving gravity. When looking for UV completions of the SM the following remarks are relevant: there are several spin $1/2$ and spin 1 degrees of freedom, but only one spin 0. If there are more, the present experimental evidence requires a hierarchy of VEVs which,

once again, is a serious fine-tuning problem. Why are all mixings small? Is it accidental or systematic (i.e. a new symmetry)? The real problem when dealing with UV completions is that one model is falsifiable, but an endless stream of them is not.

Here, we return to the "more and more scales" scenario. Even in this case it would be an error to believe that rigour is the enemy of simplicity. On the contrary, we find it confirmed by numerous examples that the rigorous method is at the same time simpler and more easily comprehended. We need a consistent theoretical framework in which deviations from the SM (or NextSM) predictions can be calculated (on average, for every 20 bogus hypotheses you test, one of them will give you a p of < 0.05). Such a framework should be applicable to comprehensively describe measurements in all sectors of particle physics: LHC Higgs measurements, past EWPD, etc.

In this section we revised a theory defined to be the SM augmented with the inclusion of higher dimensional operators (dim > 4); this theory (let's call it Th1) is not strictly renormalisable since, order by order, the number of ultraviolet (UV) divergences increases even if, order by order, they can be removed. Th1 is standalone and makes predictions, not only at lowest order (LO). Although workable to all orders, Th1 fails above a certain scale, Λ_1, because a) the perturbative expansion, in E/Λ, breaks down and b) unitarity is violated. Above Λ_1 we are forced to abandon Th1.

Consider any BSM model that is strictly renormalisable and respects unitarity and call it Th2; its parameters can be fixed by comparison with data, while masses of heavy states are presently unknown. Th1 and Th2 differ in the UV but must have the same infrared (IR) behaviour.

Consider now the whole set of data below Λ_1. Th1 should be able to explain them by fitting Wilson coefficients, Th2 should be able to explain the data adjusting the masses of heavy states (as SM did with the Higgs mass at LEP). Goodness of both explanations is crucial in understanding how well Th1 and Th2 match and how reasonable it is to use Th1 instead of the full Th2, see Ref. [83]. It is worth noting that, to a large extent Th2 is "suggested" by the comparison of Th1 and data.

The next question is: does Th2 explain all observations? Possibly not, but it should be able to explain something more than Th1. In any case, both Th1 and Th2 should be formulated at least at next-to-leading order (NLO) with UV divergences removed and, whenever possible, with Lagrangian parameters traded for experimental data.

We could now define Th3 as Th2 augmented with its own higher dimensional operators, and valid up to a scale Λ_2.

The construction of the SMEFT, to all orders, is not based on assumptions on the size of the Wilson coefficients of the higher dimensional operators; restricting to a particular UV case is not an integral part of a general SMEFT treatment and various cases can be considered after the general calculation is performed. Of course, if the value of Wilson coefficients in broad UV scenarios could be inferred in general this would be of significant scientific

value.

To summarise: constructing SMEFT is based on the fact that experiments occur at finite energy and "measure" an effective action $S^{\text{eff}}(\Lambda)$; whatever QFT should give low energy $S^{\text{eff}}(\Lambda)$, $\forall \Lambda < \infty$. One also assumes that there is no fundamental scale above which $S^{\text{eff}(\Lambda)}$ is not defined [29] and $S^{\text{eff}}(\Lambda)$ loses its predictive power if a process at $E = \Lambda$ requires ∞ renormalised parameters [30].

Extending the kappa framework should be seen as expressing the κ-parameters in terms of coefficients in the SM effective field theory (SMEFT), remembering that SMEFT converges to SM in the limit of zero Wilson coefficients, but SMEFT and SM are different theories in the UV.

7.4. Theoretical uncertainties

There is now an overall consensus on having a "truncation" error in SMEFT, and the recommendation is to quote it separately, as for example is common practice among experimentalists for different kind of systematic or statistical uncertainties. The reason for doing that is that this error is strongly model dependent, differently from other ones.

Let us refer to the case when we observe some deviation from the SM. Then, if the experimental precision allows, we could be able to test loop corrections and/or dim = 8 effects. In this case we can say that there is already strong evidence that NLO SMEFT provides non-negligible corrections, which are relevant for per-mille/few percent constraints. As it is always the case, if one works at LO and a tiny deviation is found, this deviation could be due to new physics or to missing higher orders. For a given observable one can compute the deviation and the corresponding probability distribution function (pdf) with the result that the LO pdf differs from the NLO pdf at the level required by the projected precision.

Of course, one should also consider the case where no deviation from the SM is observed and limits on the dim = 6 coefficients are set through a LO procedure. Also in this case loops should not be neglected if one wants to constrain a specific UV model, or if experimental data at widely different scales are to be combined into a single fit.

The SMEFT framework is useful because one can set limits on the effective coefficients in a model-independent way [70]. This is why SMEFT in the bottom-up approach is so useful: we do not know what the tower of UV completions is (or if it exists at all) but we can formulate the SMEFT and perform calculations with it without needing to know what happens at arbitrarily high scales. On the other hand, in the top-down approach (Sect. 7.2.1), interpreting such limits as bounds on UV models does require some assumption of the UV dynamics [121].

Unless we start observing deviations, any phenomenological "dim = 6" approach is a reasonable starting point to describe limits on SM deviations. While this outcome is much less desirable than dealing with a consistent SMEFT it is important to recognize that the

difference relates to the possibility of including theory uncertainties. SMEFT can be used in LHC Higgs physics as long as we do not see new resonances. It allows us to describe kinematic distributions and to include EW corrections. An important question to answer is on theory uncertainties when linking SMEFT to full, (weakly interacting) BSM models.

8. Prospects for Run II

From the extraordinarily successful and well-established kappa-framework we know that measurements of Higgs couplings at the level of several percent can be expected from the upcoming LHC run(s). Towards higher luminosity the Higgs couplings to weak bosons will likely be the best-measured also because the theoretical uncertainties linked to the corresponding LHC production cross sections are well under control.

The increase in LHC beam energy from 8 TeV to 13 TeV (or more) will have a significant impact on the physics reach of ATLAS and CMS. In addition, the experiments will be accumulating 10 or 100 times more data. A multi-TeV particle produced via gluon fusion will see an increase in the parton luminosity by one or two orders of magnitude relative to 7 TeV collisions. The jump in energy will enable precision measurements of Higgs boson properties and SM processes that will either help to elucidate the nature of the newly discovered particle or exclude a large set of possible alternatives to the standard model.

Precise performance assessments at 13 TeV center of mass energy and with the new upgraded detector (or with the envisaged upgrade that will happen in the future shutdown) do not exist. Only extrapolations from 7 and 8 TeV results with the detector and analyses for the Run 1 data are available.

In this Section only the results from CMS will be shown [146]. The CMS results are extrapolated to larger datasets of 300 and 3000 fb^{-1} and a center-of-mass energy of 14 TeV by scaling signal and background event yields accordingly. In order to study the precision of future measurements, a number of assumptions are made. As stated before, the extrapolations are done not considering the future detector upgrade, but assuming the same level of detector and trigger performances achieved with the detector in the 2012 data-taking period. Extrapolations are presented for two uncertainty scenarios. In Scenario 1, all systematic uncertainties are left unchanged. In Scenario 2, the theoretical uncertainties are scaled by a factor of $1/2$, while other systematic uncertainties are scaled by the inverse square root of the integrated luminosity. The comparison of the two uncertainty scenarios indicates a range of possible future measurements. The extrapolation without theoretical uncertainties is also presented as Scenario 3, to illustrate the importance of reducing those uncertainties in the future. Systematic uncertainties are inputs to the fits. They can be further constraint by the data when extracting the signal strength, coupling modifier or ratios of such. Similar extrapolations have been discussed in Ref. [146].

The estimated precision on the measurements of the signal strength for a SM-like Higgs

boson is presented in Fig. 23. The projections assume $\sqrt{s} = 14\ TeV$ and an integrated luminosity of 300 fb^{-1} (top) and 3000 fb^{-1} (middle and bottom), with and without the theoretical uncertainty. The projections are obtained with the three uncertainty scenarios described above.

The huge improvements that the detector upgrades will provide in terms of detection efficiency and resolution (efficiencies could easily double for some of the processes and resolution will be improved considerably [146]), the new methods to control the background and analyse the data that will be introduced, and the addition of more Higgs channels in the extraction of the couplings. All these will contribute to reach a much smaller uncertainty on the Higgs couplings. We think that at least a factor of 2 could be gained from the one presented in this section. Moreover, an additional improvement will come from the combination of the data from ATLAS and CMS experiments, as it has been demonstrated in the first part of this report for the Run 1 analysis.

9. Conclusions

Understanding the Higgs properties is a pillar of the present paradigm. In this review we discussed the frameworks adopted during Run 1 at LHC as well as the experimental results. Understanding that the main accent should be put on observables (i.e. quantities related to an S-matrix) is important, and mapping those observables to a Lagrangian is a truly subtle affair, that we must understand and that cannot really be demoted.

The Higgs boson production and decay rates measured by ATLAS and CMS have been combined within the context of different generic parameterisations, e.g. one based on ratios of coupling modifiers. The data are consistent with the Standard Model predictions for all parameterisations considered.

Are we expecting new revolutions and do we want them out as soon as possible? This attitude to physics is associated with the modern era and it is not new [f]. Most approaches are subjective, model-dependent, and uncertain. One simply cannot promote them to something that will reliably lead us to the next discovery in particle physics.

The desire to "abandon all the existing knowledge" is in no way new. It was surely common among physicists before the war, see Ref. [147]. "The task is, not so much to see what no one has yet seen; but to think what nobody has yet thought, about that which everybody sees" (E. Schroedinger). In our view the problem is not how to imagine wild scenarios, but rather how to arrive at the correct scenario by making only small steps, without having to make unreasonable assumptions (see Gerard 't Hooft's contribution in Ref. [148]). We have the Standard Model of particle physics with coupling strengths that we do not know how to derive, but which can be measured accurately.

[f] See http://motls.blogspot.it/2016/08/modern-obsession-with-permanent.html

In this report we have discussed not only the current framework for Run 1 studies, but we have also reviewed a study of potential generalisations, such as the SMEFT, with the belief that when it comes to the choice of the dynamics, quantum field theory will be the essential framework for effective theories.

Acknowledgments

We acknowledge important discussions with Tiziano Camporesi, Andrè David and Gino Isidori.

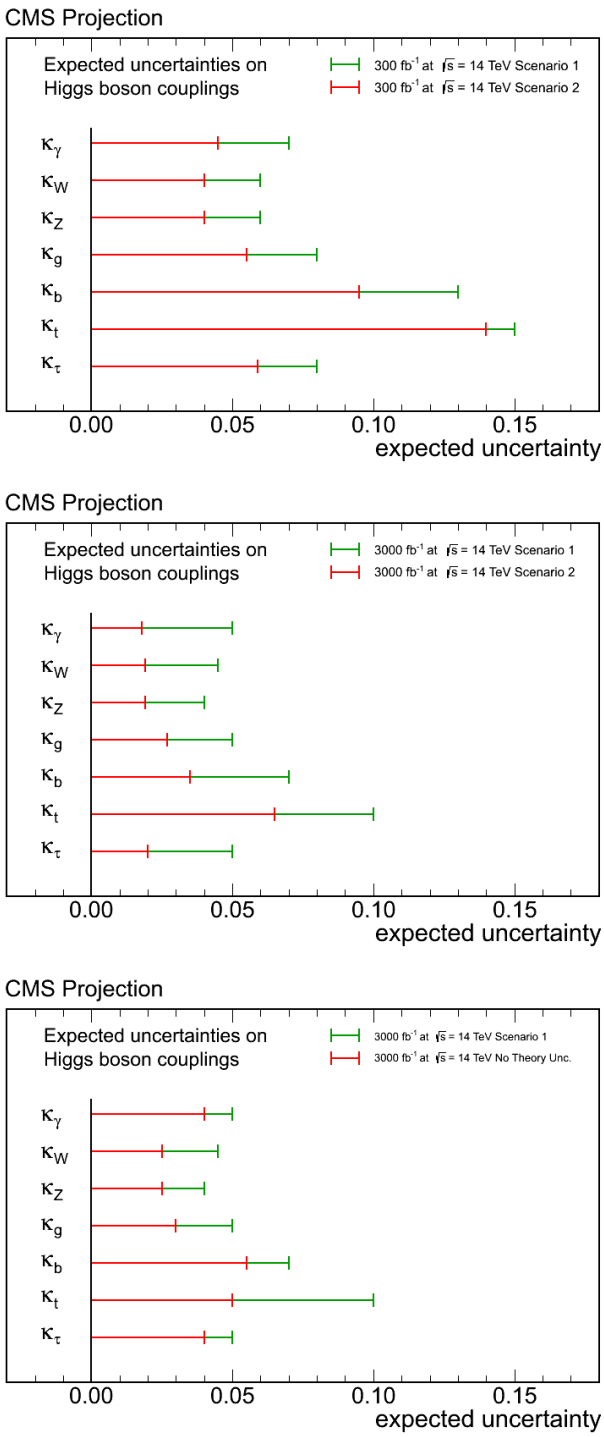

Fig. 23: Estimated precision on the measurements of the signal strength for a SM-like Higgs boson. The projections assume $\sqrt{s} = 14\ TeV$ and an integrated luminosity of 300 fb^{-1} (top), 3000 fb^{-1} (middle) and assuming no theoretical uncertainty (bottom).The projections are obtained with the three uncertainty scenarios described in the text.

References

1. F. Englert and R. Brout, *Phys. Rev. Lett.* **13**, 321 (1964), doi:10.1103/PhysRevLett.13.321. (3)
2. P. W. Higgs, *Phys. Rev. Lett.* **13**, 508 (1964), doi:10.1103/PhysRevLett.13.508. (3)
3. G. Guralnik, C. Hagen and T. Kibble, *Phys. Rev. Lett.* **13**, 585 (1964), doi:10.1103/PhysRevLett.13.585. (3)
4. P. W. Higgs, *Phys. Rev.* **145**, 1156 (1966), doi:10.1103/PhysRev.145.1156. (3)
5. T. Kibble, *Phys. Rev.* **155**, 1554 (1967), doi:10.1103/PhysRev.155.1554. (3)
6. ATLAS Collaboration (G. Aad *et al.*), *Phys. Lett.* **B716**, 1 (2012), arXiv:1207.7214 [hep-ex], doi:10.1016/j.physletb.2012.08.020. (3)
7. CMS Collaboration (S. Chatrchyan *et al.*), *Phys. Lett.* **B716**, 30 (2012), arXiv:1207.7235 [hep-ex], doi:10.1016/j.physletb.2012.08.021. (3)
8. ATLAS, CMS Collaboration (G. Aad *et al.*), *JHEP* **08**, 045 (2016), arXiv:1606.02266 [hep-ex], doi:10.1007/JHEP08(2016)045. (3, 10, 17, 19, 20, 21, 23, 24, 25, 26, 27, 28, 29, 30, 32, 33)
9. LHC Higgs Cross Section Working Group Collaboration (S. Dittmaier *et al.*) (2011), arXiv:1101.0593 [hep-ph], doi:10.5170/CERN-2011-002. (3, 6, 7, 34)
10. S. Dittmaier *et al.* (2012), arXiv:1201.3084 [hep-ph], doi:10.5170/CERN-2012-002. (3, 6, 7, 34)
11. G. Passarino, C. Sturm and S. Uccirati, *Nucl.Phys.* **B834**, 77 (2010), arXiv:1001.3360 [hep-ph], doi:10.1016/j.nuclphysb.2010.03.013. (6)
12. S. Goria, G. Passarino and D. Rosco, *Nucl.Phys.* **B864**, 530 (2012), arXiv:1112.5517 [hep-ph], doi:10.1016/j.nuclphysb.2012.07.006. (6, 46)
13. LHC Higgs Cross Section Working Group Collaboration (S. Heinemeyer *et al.*) (2013), arXiv:1307.1347 [hep-ph], doi:10.5170/CERN-2013-004. (6, 7, 8, 9, 41)
14. A. Djouadi, J. Kalinowski and M. Spira, *Comput. Phys. Commun.* **108**, 56 (1998), arXiv:hep-ph/9704448 [hep-ph], doi:10.1016/S0010-4655(97)00123-9. (6)
15. A. Bredenstein, A. Denner, S. Dittmaier and M. M. Weber, Precision calculations for H $\to$ WW/ZZ $\to$4fermions with PROPHECY4f, in *Proceedings, International Linear Collider Workshop (LCWS07 and ILC07): Hamburg , Germany, May 30-June 3, 2007, Vol.1-2*, (2007), pp. 150–154. arXiv:0708.4123 [hep-ph]. (6)
16. M. Gonzalez-Alonso, A. Greljo, G. Isidori and D. Marzocca (2015), arXiv:1504.04018 [hep-ph]. (6)
17. A. Greljo, G. Isidori, J. M. Lindert and D. Marzocca, *Eur. Phys. J.* **C76**, 158 (2016), arXiv:1512.06135 [hep-ph], doi:10.1140/epjc/s10052-016-4000-5. (6, 43, 45)
18. M. Bordone, A. Greljo, G. Isidori, D. Marzocca and A. Pattori, *Eur. Phys. J.* **C75**, 385 (2015), arXiv:1507.02555 [hep-ph], doi:10.1140/epjc/s10052-015-3611-6. (6, 43, 45)
19. A. David and G. Passarino, *Rev. Phys.* **1**, 13 (2016), arXiv:1510.00414 [hep-ph], doi:10.1016/j.revip.2016.01.001. (6, 43, 45, 46, 47)
20. T. ALEPH, DELPHI, L3, OPAL, S. Collaborations, the LEP Electroweak Working Group, the SLD Electroweak and H. F. Groups, *Phys. Rept.* **427**, 257 (2006), hep-ex/0509008. (6, 10)
21. ATLAS, CMS Collaboration (G. Aad *et al.*), *Phys. Rev. Lett.* **114**, 191803 (2015), arXiv:1503.07589 [hep-ex], doi:10.1103/PhysRevLett.114.191803. (7, 9, 17, 18)
22. J. Alwall, R. Frederix, S. Frixione, V. Hirschi, F. Maltoni, O. Mattelaer, H. S. Shao, T. Stelzer, P. Torrielli and M. Zaro, *JHEP* **07**, 079 (2014), arXiv:1405.0301 [hep-ph], doi:10.1007/JHEP07(2014)079. (8)
23. R. Harlander, M. Kramer and M. Schumacher (2011), arXiv:1112.3478 [hep-ph]. (8)
24. ATLAS Collaboration (G. Aad *et al.*), *Eur. Phys. J.* **C76**, 6 (2016), arXiv:1507.04548 [hep-ex], doi:10.1140/epjc/s10052-015-3769-y. (10, 17)
25. CMS Collaboration (V. Khachatryan *et al.*), *Eur. Phys. J.* **C75**, 212 (2015), arXiv:1412.8662

[hep-ex], doi:10.1140/epjc/s10052-015-3351-7. (10, 17, 18)
26. LHC Higgs Cross Section Working Group Collaboration (A. David *et al.*) (2012), arXiv:1209.0040 [hep-ph]. (10, 14, 41)
27. M. B. Einhorn and J. Wudka, *Nucl.Phys.* **B876**, 556 (2013), arXiv:1307.0478 [hep-ph], doi:10.1016/j.nuclphysb.2013.08.023. (11, 49, 50)
28. G. Passarino, NLO Standard model effective field theory for Higgs and EW precision data, in *13th DESY Workshop on Elementary Particle Physics: Loops and Legs in Quantum Field Theory (LL2016) Leipzig, Germany, April 24-29, 2016*, (2016). arXiv:1607.01236 [hep-ph]. (11, 42, 49, 50)
29. K. Costello, Renormalization and Effective Field Theory Mathematical Surveys and Monographs Volume 170, American Mathematical Society, (2011). (11, 57)
30. J. Preskill, *Annals Phys.* **210**, 323 (1991), doi:10.1016/0003-4916(91)90046-B. (11, 57)
31. M. Ghezzi, R. Gomez-Ambrosio, G. Passarino and S. Uccirati (2015), arXiv:1505.03706 [hep-ph]. (11, 44, 47)
32. C. Hartmann and M. Trott (2015), arXiv:1505.02646 [hep-ph]. (11, 42, 47)
33. C. Hartmann and M. Trott, *Phys. Rev. Lett.* **115**, 191801 (2015), arXiv:1507.03568 [hep-ph], doi:10.1103/PhysRevLett.115.191801. (11, 47)
34. G. Passarino and M. Trott, The Standard Model Effective Field Theory and Next to Leading Order LHCHXSWG-DRAFT-INT-2016-005, https://cds.cern.ch/record/2138031, (2016). (11, 51)
35. R. Gauld, B. D. Pecjak and D. J. Scott (2016), arXiv:1607.06354 [hep-ph]. (11)
36. P. Artoisenet *et al.*, *JHEP* **11**, 043 (2013), arXiv:1306.6464 [hep-ph], doi:10.1007/JHEP11(2013)043. (11)
37. F. Demartin, F. Maltoni, K. Mawatari, B. Page and M. Zaro, *Eur. Phys. J.* **C74**, 3065 (2014), arXiv:1407.5089 [hep-ph], doi:10.1140/epjc/s10052-014-3065-2. (11)
38. A. Falkowski, B. Fuks, K. Mawatari, K. Mimasu, F. Riva and V. sanz, *Eur. Phys. J.* **C75**, 583 (2015), arXiv:1508.05895 [hep-ph], doi:10.1140/epjc/s10052-015-3806-x. (11)
39. ATLAS Collaboration (doi:10.1140/epjc/s10052-015-3806-x), *Phys. Rev. D* **91**, 012006 (2015), arXiv:1408.5191 [hep-ex], doi:10.1103/PhysRevD.91.012006. (12)
40. CMS Collaboration (doi:10.1103/PhysRevD.91.012006), *Phys. Rev. D* **89**, 092007 (2014), arXiv:1312.5353 [hep-ex], doi:10.1103/PhysRevD.89.092007. (12, 18)
41. ATLAS Collaboration (doi:10.1103/PhysRevD.89.092007), *Phys. Rev. D* **90**, 112015 (2014), arXiv:1408.7084 [hep-ex], doi:10.1103/PhysRevD.90.112015. (12)
42. CMS Collaboration (doi:10.1103/PhysRevD.90.112015), *Eur. Phys. J. C* **74**, 3076 (2014), arXiv:1407.0558 [hep-ex], doi:10.1140/epjc/s10052-014-3076-z. (12)
43. ATLAS Collaboration (doi:10.1140/epjc/s10052-014-3076-z), *Phys. Rev. D* **92**, 012006 (2015), arXiv:1412.2641 [hep-ex], doi:10.1103/PhysRevD.92.012006. (13)
44. ATLAS Collaboration (doi:10.1103/PhysRevD.92.012006), *JHEP* **08**, 137 (2015), arXiv:1506.06641 [hep-ph], doi:10.1007/JHEP08(2015)137. (13)
45. CMS Collaboration (doi:10.1007/JHEP08(2015)137), *JHEP* **01**, 096 (2014), arXiv:1312.1129 [hep-ex], doi:10.1007/JHEP01(2014)096. (13)
46. ATLAS Collaboration (doi:10.1007/JHEP01(2014)096), *JHEP* **04**, 117. (13)
47. CMS Collaboration (117), *JHEP* **05**, 104 (2014), arXiv:1401.5041 [hep-ex], doi:10.1007/JHEP05(2014)104. (13)
48. ATLAS Collaboration (doi:10.1007/JHEP05(2014)104), *JHEP* **01**, 069 (2015), arXiv:1409.6212 [hep-ex], doi:10.1007/JHEP01(2015)069. (13)
49. CMS Collaboration (doi:10.1007/JHEP01(2015)069), *Phys. Rev. D* **89**, 012003 (2014), arXiv:1310.3687 [hep-ex], doi:10.1103/PhysRevD.89.012003. (13)
50. CMS
Collaboration (V. Khachatryan *et al.*), *Phys. Rev.* **D92**, 032008 (2015), arXiv:1506.01010

[hep-ex], doi:10.1103/PhysRevD.92.032008. (13)
51. ATLAS Collaboration (doi:10.1103/PhysRevD.92.032008), *Eur. Phys. J. C* **75**, 349 (2015), arXiv:1503.05066 [hep-ex], doi:10.1140/epjc/s10052-015-3543-1. (14)
52. ATLAS Collaboration (doi:10.1140/epjc/s10052-015-3543-1), *Phys. Lett. B* **749**, 519 (2015), arXiv:1506.05988 [hep-ex], doi:10.1016/j.physletb.2015.07.079. (14)
53. ATLAS Collaboration (doi:10.1016/j.physletb.2015.07.079), *Phys. Lett. B* **740**, 222 (2015), arXiv:1409.3122 [hep-ex], doi:10.1016/j.physletb.2014.11.049. (14)
54. CMS Collaboration (doi:10.1016/j.physletb.2014.11.049), *JHEP* **05**, 145. (14)
55. CMS Collaboration (145), *JHEP* **09**, 087 (2014), arXiv:1408.1682 [hep-ex], doi:10.1007/JHEP09(2014)087. (14)
56. ATLAS Collaboration (doi:10.1007/JHEP09(2014)087), *Phys. Lett. B* **738**, 68 (2014), arXiv:1406.7663 [hep-ex], doi:10.1016/j.physletb.2014.09.008. (14)
57. CMS Collaboration (doi:10.1016/j.physletb.2014.09.008), *Phys. Lett. B* **744**, 184 (2015), arXiv:1410.6679 [hep-ex], doi:10.1016/j.physletb.2015.03.048. (14)
58. R. Bonciani, G. Degrassi and A. Vicini, *JHEP* **11**, 095 (2007), arXiv:0709.4227 [hep-ph], doi:10.1088/1126-6708/2007/11/095. (15)
59. D. A. Ross and M. J. G. Veltman, *Nucl. Phys.* **B95**, 135 (1975), doi:10.1016/0550-3213(75)90485-X. (15)
60. M. Boggia, R. Gomez-Ambrosio and G. Passarino, *JHEP* **05**, 162 (2016), arXiv:1603.03660 [hep-ph], doi:10.1007/JHEP05(2016)162. (16, 48)
61. A. Freitas, D. Lopez-Val and T. Plehn (2016), arXiv:1607.08251 [hep-ph]. (16, 48)
62. I. Low, J. Lykken and G. Shaughnessy, *Phys. Rev.* **D86**, 093012 (2012), arXiv:1207.1093 [hep-ph], doi:10.1103/PhysRevD.86.093012. (17)
63. H. Georgi and M. Machacek, *Nucl. Phys.* **B262**, 463 (1985), doi:10.1016/0550-3213(85)90325-6. (17)
64. ATLAS Collaboration (G. Aad *et al.*), *Phys. Rev.* **D90**, 052004 (2014), arXiv:1406.3827 [hep-ex], doi:10.1103/PhysRevD.90.052004. (17, 18)
65. J. Ellis and T. You, *JHEP* **06**, 103 (2013), arXiv:1303.3879 [hep-ph], doi:10.1007/JHEP06(2013)103. (33)
66. C. Englert, R. Kogler, H. Schulz and M. Spannowsky (2015), arXiv:1511.05170 [hep-ph]. (34)
67. C. Englert, A. Freitas, M. M. Muhlleitner, T. Plehn, M. Rauch, M. Spira and K. Walz, *J. Phys.* **G41**, 113001 (2014), arXiv:1403.7191 [hep-ph], doi:10.1088/0954-3899/41/11/113001. (34)
68. J. Ellis, V. Sanz and T. You, *JHEP* **03**, 157 (2015), arXiv:1410.7703 [hep-ph], doi:10.1007/JHEP03(2015)157. (34)
69. A. Buckley, C. Englert, J. Ferrando, D. J. Miller, L. Moore, M. Russell and C. D. White, *JHEP* **04**, 015 (2016), arXiv:1512.03360 [hep-ph], doi:10.1007/JHEP04(2016)015. (34)
70. L. Berthier and M. Trott (2015), arXiv:1502.02570 [hep-ph]. (35, 47, 57)
71. L. Berthier, M. Bjorn and M. Trott (2016), arXiv:1606.06693 [hep-ph]. (35, 37)
72. J. de Blas, M. Ciuchini, E. Franco, D. Ghosh, S. Mishima, M. Pierini, L. Reina and L. Silvestrini, *Nucl. Part. Phys. Proc.* **273-275**, 834 (2016), arXiv:1410.4204 [hep-ph], doi:10.1016/j.nuclphysbps.2015.09.128. (35)
73. C. Englert, O. Mattelaer and M. . Spannowsky, *Phys. Lett.* **B756**, 103 (2016), arXiv:1512.03429 [hep-ph], doi:10.1016/j.physletb.2016.02.074. (35)
74. U. Langenegger, M. Spira and I. Strebel (2015), arXiv:1507.01373 [hep-ph]. (35)
75. M. Spira, *JHEP* **10**, 026 (2016), arXiv:1607.05548 [hep-ph], doi:10.1007/JHEP10(2016)026. (35)
76. W. Bizon, M. Gorbahn, U. Haisch and G. Zanderighi (2016), arXiv:1610.05771 [hep-ph]. (35)

77. G. Degrassi, P. P. Giardino, F. Maltoni and D. Pagani (2016), arXiv:1607.04251 [hep-ph]. (36)
78. F. Bishara, U. Haisch, P. F. Monni and E. Re (2016), arXiv:1606.09253 [hep-ph]. (36)
79. A. V. Gritsan, R. Röntsch, M. Schulze and M. Xiao, *Phys. Rev.* **D94**, 055023 (2016), arXiv:1606.03107 [hep-ph], doi:10.1103/PhysRevD.94.055023. (36)
80. F. Demartin, B. Maier, F. Maltoni, K. Mawatari and M. Zaro (2016), arXiv:1607.05862 [hep-ph]. (36)
81. B. Hespel, F. Maltoni and E. Vryonidou, *JHEP* **10**, 016 (2016), arXiv:1606.04149 [hep-ph], doi:10.1007/JHEP10(2016)016. (36)
82. M. Bjorn and M. Trott (2016), arXiv:1606.06502 [hep-ph]. (37)
83. J. Brehmer, A. Freitas, D. Lopez-Val and T. Plehn, *Phys. Rev.* **D93**, 075014 (2016), arXiv:1510.03443 [hep-ph], doi:10.1103/PhysRevD.93.075014. (37, 47, 48, 56)
84. A. Biekotter, J. Brehmer and T. Plehn (2016), arXiv:1602.05202 [hep-ph]. (37, 48)
85. A. Banfi, A. Martin and V. Sanz, *JHEP* **08**, 053 (2014), arXiv:1308.4771 [hep-ph], doi:10.1007/JHEP08(2014)053. (37)
86. M. Buschmann, C. Englert, D. Goncalves, T. Plehn and M. Spannowsky, *Phys. Rev.* **D90**, 013010 (2014), arXiv:1405.7651 [hep-ph], doi:10.1103/PhysRevD.90.013010. (37)
87. N. Kauer and G. Passarino, *JHEP* **1208**, 116 (2012), arXiv:1206.4803 [hep-ph], doi:10.1007/JHEP08(2012)116. (37)
88. N. Kauer, *Mod.Phys.Lett.* **A28**, 1330015 (2013), arXiv:1305.2092 [hep-ph], doi:10.1142/S0217732313300152. (37)
89. F. Caola and K. Melnikov, *Phys.Rev.* **D88**, 054024 (2013), arXiv:1307.4935 [hep-ph], doi:10.1103/PhysRevD.88.054024. (37, 38)
90. G. Passarino, *Eur. Phys. J.* **C74**, 2866 (2014), arXiv:1312.2397 [hep-ph], doi:10.1140/epjc/s10052-014-2866-7. (37, 39)
91. L. J. Dixon and Y. Li, *Phys. Rev. Lett.* **111**, 111802 (2013), arXiv:1305.3854 [hep-ph], doi:10.1103/PhysRevLett.111.111802. (38)
92. J. M. Campbell, R. K. Ellis and C. Williams, *PoS* **LL2014**, 008 (2014), arXiv:1408.1723 [hep-ph]. (38)
93. J. M. Campbell, R. K. Ellis and C. Williams (2013), arXiv:1311.3589 [hep-ph]. (38)
94. ATLAS Collaboration (G. Aad *et al.*), *Eur. Phys. J.* **C75**, 335 (2015), arXiv:1503.01060 [hep-ex], doi:10.1140/epjc/s10052-015-3542-2. (38)
95. CMS Collaboration (V. Khachatryan *et al.*), *Phys. Lett.* **B736**, 64 (2014), arXiv:1405.3455 [hep-ex], doi:10.1016/j.physletb.2014.06.077. (38)
96. CMS Collaboration (V. Khachatryan *et al.*), *JHEP* **09**, 051 (2016), arXiv:1605.02329 [hep-ex], doi:10.1007/JHEP09(2016)051. (38)
97. F. Cascioli, T. Gehrmann, M. Grazzini, S. Kallweit, P. Maierhöfer, A. von Manteuffel, S. Pozzorini, D. Rathlev, L. Tancredi and E. Weihs, *Phys. Lett.* **B735**, 311 (2014), arXiv:1405.2219 [hep-ph], doi:10.1016/j.physletb.2014.06.056. (39)
98. F. Caola, K. Melnikov, R. Räntsch and L. Tancredi, *Phys. Rev.* **D92**, 094028 (2015), arXiv:1509.06734 [hep-ph], doi:10.1103/PhysRevD.92.094028. (39)
99. A. von Manteuffel and L. Tancredi, *JHEP* **06**, 197 (2015), arXiv:1503.08835 [hep-ph], doi:10.1007/JHEP06(2015)197. (39)
100. M. Grazzini, S. Kallweit and D. Rathlev, *Phys. Lett.* **B750**, 407 (2015), arXiv:1507.06257 [hep-ph], doi:10.1016/j.physletb.2015.09.055. (39)
101. K. Melnikov and M. Dowling, *Phys. Lett.* **B744**, 43 (2015), arXiv:1503.01274 [hep-ph], doi:10.1016/j.physletb.2015.03.030. (39)
102. J. M. Campbell and R. K. Ellis, *JHEP* **04**, 030 (2015), arXiv:1502.02990 [hep-ph], doi:10.1007/JHEP04(2015)030. (39)
103. G. Passarino and M. Trott, The Standard Model Effective Field Theory and Next to Leading

Order (2016). arXiv:1610.08356 [hep-ph]. (41)
104. G. Passarino (2016), arXiv:1610.09618 [hep-ph]. (41)
105. LHC Higgs Cross Section Working Group Collaboration (D. de Florian *et al.*) (2016), arXiv:1610.07922 [hep-ph]. (41)
106. D. Y. Bardin, M. Grunewald and G. Passarino (1999), arXiv:hep-ph/9902452. (42)
107. D. Y. Bardin and G. Passarino (1998), arXiv:hep-ph/9803425 [hep-ph]. (42)
108. G. Isidori, A. Greljo, J. Lindert, D. Marzocca and G. Passarino, Pseudo-observables in Higgs physics LHCHXSWG-DRAFT-INT-2016-004, https://cds.cern.ch/record/2138023, (2016). (43, 45, 53)
109. M. Gonzalez-Alonso, A. Greljo, G. Isidori and D. Marzocca, *Eur. Phys. J.* **C75**, 128 (2015), arXiv:1412.6038 [hep-ph], doi:10.1140/epjc/s10052-015-3345-5. (43, 45)
110. P. A. Grassi, B. A. Kniehl and A. Sirlin, *Phys. Rev. Lett.* **86**, 389 (2001), arXiv:hep-th/0005149, doi:10.1103/PhysRevLett.86.389. (46)
111. H. Weldon, *Phys.Rev.* **D14**, 2030 (1976), doi:10.1103/PhysRevD.14.2030. (46)
112. A. Denner, S. Dittmaier, M. Roth and L. H. Wieders, *Phys. Lett.* **B612**, 223 (2005), arXiv:hep-ph/0502063 [hep-ph], doi:10.1016/j.physletb.2005.03.007,10.1016/j.physletb.2011.09.020, [Erratum: Phys. Lett.B704,667(2011)]. (46)
113. M. Nekrasov, *Int.J.Mod.Phys.* **A24**, 6071 (2009), arXiv:0709.3046 [hep-ph], doi:10.1142/S0217751X09047673. (47)
114. G. Passarino, *Phys. Lett.* **B727**, 424 (2013), arXiv:1308.0422 [hep-ph], doi:10.1016/j.physletb.2013.10.052. (47)
115. G. Buchalla, O. Cata and C. Krause, *Nucl.Phys.* **B880**, 552 (2014), arXiv:1307.5017 [hep-ph], doi:10.1016/j.nuclphysb.2014.01.018. (47)
116. J. Bain, *Eur.J.Phil.Sci.* **3**, 257 (2013), doi:10.1007/s13194-013-0067-0. (48)
117. B. Henning, X. Lu and H. Murayama, *JHEP* **01**, 023 (2016), arXiv:1412.1837 [hep-ph], doi:10.1007/JHEP01(2016)023. (48)
118. F. del Aguila, Z. Kunszt and J. Santiago, *Eur. Phys. J.* **C76**, 244 (2016), arXiv:1602.00126 [hep-ph], doi:10.1140/epjc/s10052-016-4081-1. (48)
119. B. Henning, X. Lu and H. Murayama (2016), arXiv:1604.01019 [hep-ph]. (48)
120. J. Fuentes-Martin, J. Portoles and P. Ruiz-Femenia, *JHEP* **09**, 156 (2016), arXiv:1607.02142 [hep-ph], doi:10.1007/JHEP09(2016)156. (48)
121. R. Contino, A. Falkowski, F. Goertz, C. Grojean and F. Riva (2016), arXiv:1604.06444 [hep-ph]. (48, 51, 57)
122. H. Georgi, *Ann. Rev. Nucl. Part. Sci.* **43**, 209 (1993), doi:10.1146/annurev.ns.43.120193.001233. (49, 50)
123. B. Grzadkowski, M. Iskrzynski, M. Misiak and J. Rosiek, *JHEP* **1010**, 085 (2010), arXiv:1008.4884 [hep-ph], doi:10.1007/JHEP10(2010)085. (49, 51)
124. L. Lehman and A. Martin, *JHEP* **02**, 081 (2016), arXiv:1510.00372 [hep-ph], doi:10.1007/JHEP02(2016)081. (49)
125. B. Henning, X. Lu, T. Melia and H. Murayama (2015), arXiv:1507.07240 [hep-th], doi:10.1007/s00220-015-2518-2. (49)
126. B. Henning, X. Lu, T. Melia and H. Murayama (2015), arXiv:1512.03433 [hep-ph]. (49)
127. S. Weinberg, *Phys. Lett.* **B91**, 51 (1980), doi:10.1016/0370-2693(80)90660-7. (49, 50)
128. S. R. Coleman, J. Wess and B. Zumino, *Phys. Rev.* **177**, 2239 (1969), doi:10.1103/PhysRev.177.2239. (49, 50)
129. C. G. Callan, Jr., S. R. Coleman, J. Wess and B. Zumino, *Phys. Rev.* **177**, 2247 (1969), doi:10.1103/PhysRev.177.2247. (49, 50)
130. A. Manohar and H. Georgi, *Nucl. Phys.* **B234**, 189 (1984), doi:10.1016/0550-3213(84)90231-1. (50)
131. D. B. Kaplan, Effective field theories, in *Beyond the standard model 5. Proceedings, 5th*

Conference, Balholm, Norway, April 29-May 4, 1997, (1995). arXiv:nucl-th/9506035 [nucl-th]. (50)

132. A. V. Manohar, *Lect. Notes Phys.* **479**, 311 (1997), arXiv:hep-ph/9606222 [hep-ph], doi:10.1007/BFb0104294. (50)
133. A. G. Cohen, D. B. Kaplan and A. E. Nelson, *Phys. Lett.* **B412**, 301 (1997), arXiv:hep-ph/9706275 [hep-ph], doi:10.1016/S0370-2693(97)00995-7. (50)
134. M. A. Luty, *Phys. Rev.* **D57**, 1531 (1998), arXiv:hep-ph/9706235 [hep-ph], doi:10.1103/PhysRevD.57.1531. (50)
135. J. Polchinski, Effective field theory and the Fermi surface, in *Theoretical Advanced Study Institute (TASI 92): From Black Holes and Strings to Particles Boulder, Colorado, June 3-28, 1992*, (1992). arXiv:hep-th/9210046 [hep-th]. (50)
136. I. Z. Rothstein, TASI lectures on effective field theories (2003). arXiv:hep-ph/0308266 [hep-ph]. (50)
137. W. Skiba, Effective Field Theory and Precision Electroweak Measurements, in *Physics of the large and the small, TASI 09, proceedings of the Theoretical Advanced Study Institute in Elementary Particle Physics, Boulder, Colorado, USA, 1-26 June 2009*, (2011), pp. 5–70. arXiv:1006.2142 [hep-ph]. (50)
138. C. P. Burgess, *Ann. Rev. Nucl. Part. Sci.* **57**, 329 (2007), arXiv:hep-th/0701053 [hep-th], doi:10.1146/annurev.nucl.56.080805.140508. (50)
139. E. E. Jenkins, A. V. Manohar and M. Trott, *JHEP* **1309**, 063 (2013), arXiv:1305.0017 [hep-ph], doi:10.1007/JHEP09(2013)063. (50)
140. E. E. Jenkins, A. V. Manohar and M. Trott, *Phys.Lett.* **B726**, 697 (2013), arXiv:1309.0819 [hep-ph], doi:10.1016/j.physletb.2013.09.020. (50)
141. G. Buchalla, O. Cata and C. Krause, *Nucl. Phys.* **B894**, 602 (2015), arXiv:1412.6356 [hep-ph], doi:10.1016/j.nuclphysb.2015.03.024. (50)
142. G. Buchalla, O. Cata and C. Krause, *Phys. Lett.* **B731**, 80 (2014), arXiv:1312.5624 [hep-ph], doi:10.1016/j.physletb.2014.02.015. (50)
143. B. M. Gavela, E. E. Jenkins, A. V. Manohar and L. Merlo (2016), arXiv:1601.07551 [hep-ph]. (50, 51)
144. C. Arzt, M. B. Einhorn and J. Wudka, *Nucl. Phys.* **B433**, 41 (1995), arXiv:hep-ph/9405214 [hep-ph], doi:10.1016/0550-3213(94)00336-D. (50)
145. S. Hartmann, Effective field theories, reduction and scientific explanation Studies in History and Philosophy of Modern Physics 32B, 267−304, (2001). (55)
146. CMS Collaboration, Projected Performance of an Upgraded CMS Detector at the LHC and HL-LHC: Contribution to the Snowmass Process, in *Proceedings, Community Summer Study 2013: Snowmass on the Mississippi (CSS2013): Minneapolis, MN, USA, July 29-August 6, 2013*, (2013). arXiv:1307.7135 [hep-ex]. (58, 59)
147. D. J. Gross, Oscar Klein and gauge theory, in *The Oskar Klein centenary. Proceedings, Symposium, Stockholm, Sweden, September 19-21, 1994*, (1994), pp. 94–111. arXiv:hep-th/9411233 [hep-th]. (59)
148. G. t. Hooft, S. B. Giddings, C. Rovelli, P. Nicolini, J. Mureika, M. Kaminski and M. Bleicher, The Good, the Bad, and the Ugly of Gravity and Information (2016). arXiv:1609.01725 [hep-th]. (59)